Catalysis Science & Technology

ROYAL SOCIETY OF CHEMISTRY

MINI REVIEW

View Article Online
View Journal | View Issue

Cite this: *Catal. Sci. Technol.*, 2023, **13**, 2877

Recent advances on g-C_3N_4-based Z-scheme photocatalysts for organic pollutant removal

Chunxue Li,[a] Hao Lu,*[b] Guixiang Ding,[c] Qing Li*[d] and Guangfu Liao *[c]

Received 21st February 2023,
Accepted 24th March 2023

DOI: 10.1039/d3cy00242j

rsc.li/catalysis

Graphitic carbon nitride (g-C_3N_4)-based Z-scheme photocatalysts have attracted growing interest in organic pollution removal because of their strong light absorption capacity, abundant active sites, and outstanding photocatalytic performance. This review provides a survey of the latest advances of g-C_3N_4-based Z-scheme photocatalysts for organic pollution removal, beginning with the fundamentals of g-C_3N_4-based Z-scheme photocatalysts. Subsequently, the characterization strategies and preparation approaches for g-C_3N_4-based Z-scheme photocatalysts are discussed. Various typical g-C_3N_4-based Z-scheme photocatalysts for organic pollutant degradation are described. Finally, this work provides some new insights into the major challenges, favorable circumstances, heuristic perspectives, and future development direction.

1. Introduction

Water pollution has attracted growing interest because of the rapid industrial development and expanding population.[1–6] The exploration and development of advanced technologies, such as adsorption,[7–10] electrocatalysis,[11,12] and photocatalysis[13–19] (especially visible-light-responsive photocatalysis),[20–24] are very promising for overcoming these issues. Among them, the most promising strategy is photocatalysis because of its unique advantage in simply using inexhaustible solar energy to organic pollution removal.[19,25–31] Graphitic carbon nitride (g-C_3N_4)-based materials, as one of the most up-and-coming photocatalysts, have gained dramatically growing interests in organic pollution removal owing to their easy functionalization, suitable electronic and band structure, excellent physicochemical stability and photocatalytic property.[32–47] Although great progress has been made, the photocatalytic performance of single g-C_3N_4 is still far from practical

[a] *College of Ecological Environment and Urban Construction, Fujian University of Technology, Fuzhou 350118, China*
[b] *School of Materials Science and Engineering, Suzhou University of Science and Technology, Suzhou 215009, China. E-mail: haolu@usts.edu.cn*
[c] *College of Material Engineering, Fujian Agriculture and Forestry University, Fuzhou 350002, China. E-mail: liaogf@mail2.sysu.edu.cn*
[d] *Ministry of Education Key Laboratory for the Green Preparation and Application of Functional Materials, Hubei Key Laboratory of Polymer Materials, School of Materials Science and Engineering, Hubei University, Wuhan 430062, China. E-mail: liqing@hubu.edu.cn*

Chunxue Li

Chunxue Li obtained her B.Sc. (2016) and M.S. (2019) from Jilin Normal University. She then obtained her Ph.D. from Jiangsu University. Presently, she is a Lecturer at Fujian University of Technology. Her current research focuses on the synthesis and application of semiconductor nanomaterials for photocatalytic hydrogen evolution. She has received some awards, including the Graduate Student National Scholarship, Xue Liang Scholarship, and Excellent Graduation Thesis of Jilin Normal University.

Hao Lu

Hao Lu received his Ph.D. degree in Physics from Soochow University in 2017. He is currently working at the School of Materials Science and Engineering, Suzhou University of Science and Technology, as an Associate Professor. His research interest involves the fabrication of high-performance optoelectronic devices by exploiting the morphology, surface and boundary of materials and energy bands. So far, he has published more than 60 high-profile SCI papers, such as Adv. Mater., Adv. Funct. Mater., Adv. Sci., Nano Energy, Sci. Bull., and Phys. Rev. Letters.

production demand owing to the fast electron–hole (e^-–h^+) recombination and poor light absorption capacity.[48–51] Hence, it is crucial to explore new g-C_3N_4-based photocatalysts with strong light absorption capacity and high e^-–h^+ separation for organic pollutant removal.

Guixiang Ding

Guixiang Ding received his B.S. degree from the College of Chemical Engineering at Liaoning Normal University in 2022. His current research focuses on the study of the photocatalytic CO_2 reduction and on the development of photocatalytic materials. He has published one SCI as the first author and four SCI as the second author.

To enhance the photocatalytic property of g-C_3N_4, various approaches have been proposed, *e.g.*, doping,[52,53] obtaining porous architectures,[54,55] achieving highly crystalline structures,[56] metal loading,[57,58] heterojunction construction,[59–61] exfoliation,[62,63] defect engineering,[64,65] and molecular and electronic structure engineering.[66–69] Among these approaches, the integration of two semiconductors to fabricate type-II heterojunctions is a promising method for enhancing the photocatalytic performance since the band alignment between the two semiconductors will provide high separation efficiency of the photogenerated carrier.[70,71] However, their photocatalytic activity is not significantly enhanced because of electrostatic repulsion.[72] To overcome this disadvantage, an emerging g-C_3N_4-based Z-scheme system was proposed by the Yu group[73] that created a more negative conduction band (CB) and more positive valence band (VB), and further achieved stronger photocatalytic ability.[74,75] When compared to type-II heterojunctions, the charge migration of Z-scheme systems is more favorable. Owing to their strong light absorption capacity, abundant active sites, and outstanding photocatalytic performance,[76] g-C_3N_4-based Z-scheme photocatalysts have achieved increasing attention for organic pollutant removal.

Qing Li

Qing Li obtained his B.Sc. (2012), M.S. (2015) and Ph.D. (2018) from Hubei University. Presently, he is an Associate Professor at Hubei University. His current research focuses on the synthesis and application of Ag-based catalytic materials. He has received some awards, including the Graduate Student National Scholarship, Excellent Innovation and Entrepreneurship Mentor, and others.

Guangfu Liao

Guangfu Liao received his Ph.D. degree in Material Physics & Chemistry from Sun Yat-sen University in 2020. Then, he joined the laboratory of Prof. Yi-Chun Lu at The Chinese University of Hong Kong, where he worked as a Research Associate. Subsequently, he became a Researcher at the China University of Geosciences. Now, he is a Professor at Fujian Agriculture and Forestry University. His research interests involve photo- and electrocatalysis, polymer synthesis and applications, polymer membranes, redox flow batteries, nanoporous and nanostructured materials, biomaterials, gas storage and energy conversion, and others. The broader impacts of his research include polymeric photocatalysts, polymer design and synthesis, nanostructure engineering, and biomaterials. So far, he has published more than 60 high profile SCI papers, such as Matter, Progress in Materials Science, Energy & Environmental Science, Applied Catalysis B: Environmental, Nano Energy, ACS Catalysis, Chemical Science, Small, Chemical Engineering Journal, Journal of Materials Chemistry A, Journal of Catalysis, and others. The awards he has received up to now include the National Endeavor Fellowship, Guanghua Scholarship, 2022 Journal of Materials Chemistry A Emerging Investigators, and others. He also serves as an Associate Editor for Frontiers in Energy Research, Guest Editor for Polymers, and Youth Editorial Board for Advanced Fiber Materials.

Although there have been many inspired reviews on g-C_3N_4-based photocatalysts for various applications,[32,33,71,77–88] a comprehensive review about g-C_3N_4-based Z-scheme photocatalysts for organic pollutant removal is nonexistent despite the great interest in this research topic. In this review, the fundamentals of g-C_3N_4-based Z-scheme photocatalysts are firstly discussed. Subsequently, the characterization strategies and preparation methods for g-C_3N_4-based Z-scheme photocatalysts are illustrated. Next, some typical g-C_3N_4-based Z-scheme photocatalysts for organic pollutant removal are described. Finally, this work provides some advanced insights into the major challenges, favorable circumstances, heuristic perspectives, and future development direction.

2. What are g-C_3N_4-based Z-scheme photocatalysts?

Before introducing the g-C_3N_4-based Z-scheme photocatalysts, it is crucial to fully comprehend g-C_3N_4-based type-II heterojunctions, *e.g.*, CeO_2/g-C_3N_4,[89] Co_3O_4/g-C_3N_4,[90] Cu_2O/g-C_3N_4,[91] Fe_2O_3/g-C_3N_4,[92] g-C_3N_4/g-C_3N_4,[93] h-BN/flower-ring g-C_3N_4,[94] which display outstanding photocatalytic property owing to their high separation efficiency of photogenerated charges through the band alignment.[74,95] In these type-II heterojunctions, both CB and VB potentials of semiconductor 1 are lower than those of g-C_3N_4 (Fig. 1A). The e^- in the CB of semiconductor 1 have a tendency to migrate to the CB of g-C_3N_4 owing to the band alignment. Similarly, the h^+ in the VB of g-C_3N_4 easily migrate to the VB of semiconductor 1.[96,97] Owing to the e^- and h^+ being concentrated on g-C_3N_4 and semiconductor 1, respectively, high separation efficiency of the photogenerated e^- and h^+ can be achieved through type-II heterojunctions.[32,72,98,99] However, there are still some potential problems that need to be solved. The photocatalytic activity of the charges are not significantly enhanced.[100,101] It is also very difficult for the e^- in semiconductor 1 and h^+ in g-C_3N_4 to migrate to the CB of g-C_3N_4 because of strong electrostatic repulsions, such as e^-–e^- or h^+–h^+ interactions, respectively.[74] Thus, it is critical to fabricate a new type of photocatalytic system to relieve this disadvantage.

Inspired by bionic photosynthesis, there is great potential in the development of the Z-scheme photocatalysts for enhancing photocatalytic performance.[71,102] In 2013, the Yu group reported on the first use of a direct Z-scheme mechanism to explain the outstanding photocatalytic formaldehyde (HCHO) oxidation performance over TiO_2/g-C_3N_4 hybrids.[73] Especially, the direct Z-scheme systems exhibit a structure similar to that of type-II heterojunctions (Fig. 1A), but they possess an evidently dissimilar charge migration mechanism.[103,104] The charge migration path of the direct Z-scheme photocatalysts resembles the letter "Z" (Fig. 1B), in which the e^- in g-C_3N_4 with stronger oxidation ability will integrate with the h^+ in semiconductor 1 with strong reduction ability.[105] Therefore, the e^- in semiconductor 1 with stronger reduction ability and h^+ in g-C_3N_4 with stronger oxidation ability may be retained. As a result, the photocatalytic property of the direct Z-scheme systems can be evidently enhanced. Moreover, the charge migration path of the direct Z-scheme systems is more favorable than that of type-II heterojunctions. This is because the migration of the photogenerated e^- from the CB of g-C_3N_4 to the VB of semiconductor 1 with adequate photogenerated h^+ is very favorable owing to the effective electrostatic attraction.[72] It is believed that g-C_3N_4-based Z-scheme systems exhibit faster charge transfer[101] when compared with g-C_3N_4-based type-II heterojunctions.

Until now, there have been two main types of g-C_3N_4-based Z-scheme systems, including g-C_3N_4-based direct Z-scheme (Fig. 1B) without an electron mediator and g-C_3N_4-based semiconductor–conductor–semiconductor (SCS)

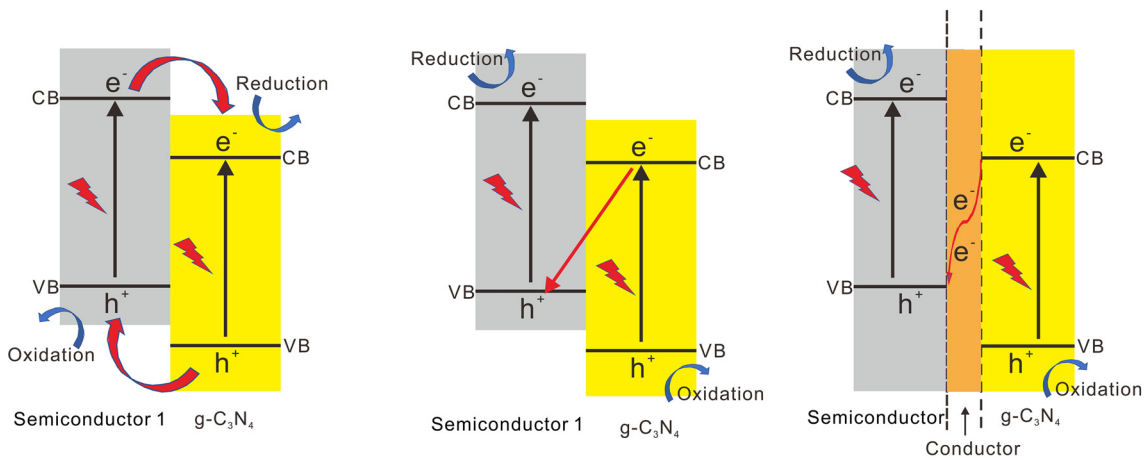

Fig. 1 Comparative analysis of the charge transfer mechanism on g-C_3N_4-based type-II heterojunctions (A), g-C_3N_4-based Z-scheme (B) and (C) g-C_3N_4-based SCS Z-scheme systems.

Z-scheme system (Fig. 1C) with an electron mediator (conductor), *e.g.*, conductive polymer, graphene, noble metal.[106,107] The g-C_3N_4-based direct Z-scheme systems (*e.g.*, TiO_2/g-C_3N_4,[73] ZnO/g-C_3N_4,[108] WO_3/g-C_3N_4,[109] Ag_3PO_4/g-C_3N_4,[110] $BiVO_4$/g-C_3N_4,[111] Bi_2WO_6/g-C_3N_4,[112] BiOCl/g-C_3N_4,[113] AgBr/g-C_3N_4 (ref. 114)) display outstanding photocatalytic performance by keeping a very negative CB and a very positive VB.[115] As for g-C_3N_4-based SCS Z-scheme systems (*e.g.*, WO_3/Cu/gC_3N_4,[116] Ag_3PO_4/Ag/g-C_3N_4,[117] CdS/Au/g-C_3N_4 (ref. 106)), a conductor acting as a mediator is utilized to link two components for more favorable migration of photogenerated carriers.[118] Moreover, the p–n Z-scheme systems (*e.g.*, C_3N_4–Pd–Cu_2O,[119] $LaFeO_3$/g-C_3N_4,[120] g-C_3N_4/$CaFe_2O_4$,[121] black phosphorus nanosheets/$FeSe_2$/g-C_3N_4 (ref. 122)) favorably formed by combining p-type and n-type materials have received increasing attention. In the comprehensive consideration of the photocatalytic activity and fabrication cost, we must compare the advantages and disadvantages of the two g-C_3N_4-based Z-scheme systems, and develop a more appropriate photocatalytic system to achieve optimal photocatalytic property. The balance of charge utilization is also vital.[123] The consumption of e^- and h^+ for redox reactions should be unified. Otherwise, the accumulation of charges may lead to the self-oxidation/reduction of the photocatalysts or the mediators.[124]

3. Characterization strategies for g-C_3N_4-based Z-scheme photocatalysts

As shown above, the Z-scheme systems exhibit similar structures with type-II heterojunctions. Therefore, it is important to prove that the charge migration mechanism occurs *via* multifarious characterization strategies, *e.g.*, self-confirmation *via* photocatalytic reactions, products, and radical species, selective photodeposition of noble metal, X-ray photoelectron spectroscopy (XPS), surface photovoltage (SPV) techniques, density function theory (DFT) calculation, and others.

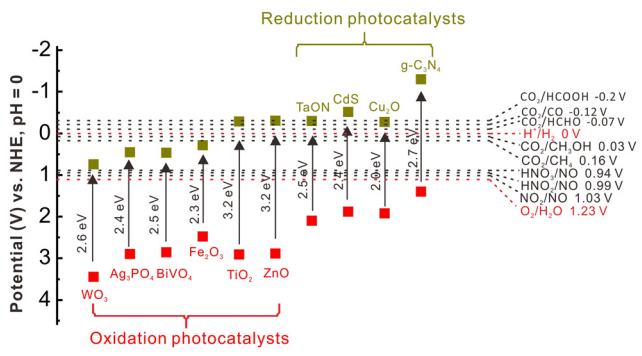

Fig. 2 Standard redox potentials of some commonly used semiconductors. Reproduced with permission from ref. 35.

3.1. Self-confirmation *via* photocatalytic reactions, products, and radical species

It is generally known that not all photogenerated charges centered on the photocatalysts' surface are utilized for the photocatalytic reaction. Typically, there are only some photogenerated e^- in a semiconductor with enough redox potential that can be utilized for photocatalytic reactions.[76,125,126] Some commonly used standard redox potentials are shown in Fig. 2. Z-scheme systems can be confirmed *via* standard redox potentials and by investigating the photocatalytic reactions, products, and radical species.

Considering the g-C_3N_4/WO_3 photocatalysts as an example, a tight contact between g-C_3N_4 and WO_3 can be found (Fig. 3A), and the individual g-C_3N_4 and WO_3 components exhibit low photocatalytic performance (Fig. 3B and C). Interestingly, the g-C_3N_4/WO_3 composites display enhanced photocatalytic performance. This phenomenon is mainly attributed to the fabrication of a direct Z-scheme system (Fig. 3D), which accelerated the separation of photogenerated e^-–h^+. The g-C_3N_4/WO_3 composites also exhibited good stability (Fig. 3E).[127] If it follows type II mechanism, the photogenerated e^- will transfer from the CB of g-C_3N_4 to the CB of WO_3. In this way, the g-C_3N_4/WO_3 composites would display reduced redox capability, which conflicts with the experimental results. Therefore, it should obey the Z-scheme direct mechanism.

We can also prove the Z-scheme mechanism through analyzing the photocatalytic products. Tao and co-workers[128] proved the successful fabrication of the g-C_3N_4/$CoTiO_3$ direct Z-scheme heterojunctions through analyzing the photocatalytic products. The single $CoTiO_3$ displayed very low photocatalytic activity due to its low reduction ability, but the single g-C_3N_4 exhibited moderate photocatalytic performance owing to its adequate reduction ability. After the successful construction of a direct Z-scheme photocatalyst, the photogenerated carrier separation efficiency and the redox ability of g-C_3N_4/$CoTiO_3$ were evidently improved. If the migration route of the photogenerated carriers follows the type-II mechanism, the photogenerated e^- would be focused on $CoTiO_3$ without adequate reduction potential, which would result in very low photocatalytic activity. Nevertheless, the experimental results unveiled that g-C_3N_4/$CoTiO_3$ exhibited enhanced photocatalytic property, suggesting that the g-C_3N_4/$CoTiO_3$ composites should follow the Z-scheme direct mechanism. This work demonstrated that the photocatalytic tests feasibly study the charge migration mechanism.

3.2. Selective photodeposition of noble metals

As for Z-scheme systems, the photogenerated charges can be efficiently separated. Photodeposition of several noble metals, *e.g.*, Au, Ag, Cu, on electron-rich areas is a promising strategy to unlock the photocatalytic reaction

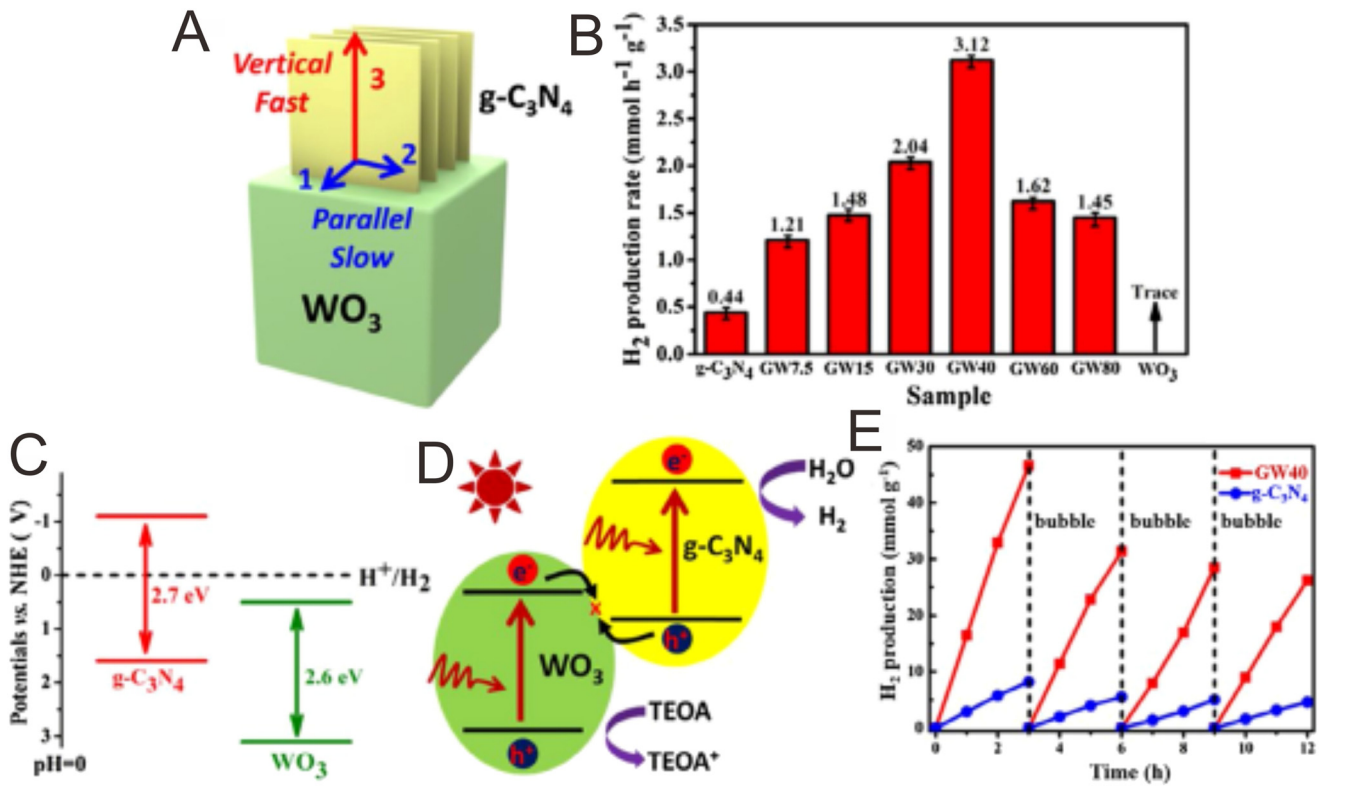

Fig. 3 (A) The growth and extension of g-C_3N_4 parallel with and perpendicular to the flat surface of the WO_3 nanocuboids. (B) Comparison of the photocatalytic H_2 production properties. (C) Band structure of g-C_3N_4 and WO_3. (D) The direct Z-scheme charge migration path in the g-C_3N_4/WO_3 composites. (E) The photocatalytic stability tests of the g-C_3N_4 and g-C_3N_4/WO_3 composites. Reproduced with permission from ref. 127.

sites.[129] On the basis of the photodeposition sites of noble metals, the charge migration route and Z-scheme mechanism can be further proved. For example, Yu and co-workers[130] proposed Fe_2O_3/g-C_3N_4 photocatalysts, which showed improved photocatalytic performance when compared with the pure Fe_2O_3 and g-C_3N_4 components. The TEM image (Fig. 4) showed that Pt nanoparticles were deposited on g-C_3N_4, but not on Fe_2O_3, suggesting that the photogenerated e^- mainly focused on g-C_3N_4. If there were no close contacts between g-C_3N_4 and Fe_2O_3, Pt nanoparticles would randomly photodeposit on g-C_3N_4 and Fe_2O_3. If it followed the type II mechanism, the Pt nanoparticles would mainly concentrate on Fe_2O_3. Instead, the Pt nanoparticles mainly concentrated on g-C_3N_4. Therefore, the Fe_2O_3/g-C_3N_4 systems should follow the Z-scheme mechanism.

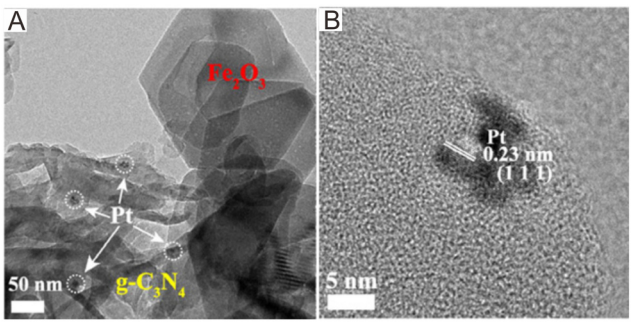

Fig. 4 (A) TEM image and (B) HRTEM image of the Fe_2O_3/g-C_3N_4 composites after photodeposition of Pt nanoparticles. Reproduced with permission from ref. 130.

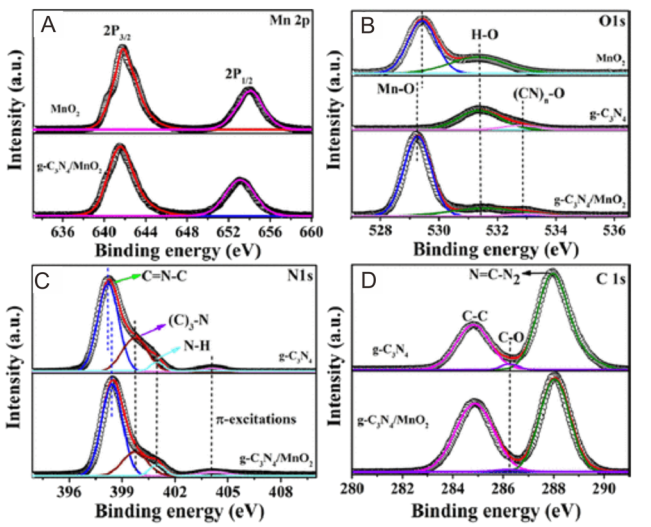

Fig. 5 XPS spectra of (A) Mn 2p, (B) O 1s, (C) N 1s, and (D) C 1s for g-C_3N_4, MnO_2, and g-C_3N_4/MnO_2. Reproduced with permission from ref. 137.

3.3. XPS characterization

XPS is a promising technique for analyzing the photocatalysts' surface chemistry,[9,131–135] and it is also used for investigating the transformations in the electronic density on the photocatalysts' surface *via* probing the shift in the binding energies.[98,136] A positive shift indicates a decrease of the electron density. Therefore, a shift in the binding energy can be used to study the migration path of photogenerated e^-. For g-C_3N_4/MnO_2,[137] the Mn 2p spectrum of the MnO_2 nanosheets (Fig. 5A) displayed two main peaks located at 641.9 and 654.0 eV, corresponding to Mn $2P_{3/2}$ and Mn $2P_{1/2}$, respectively, which shifted to 641.6 and 653.7 eV. However, the pure g-C_3N_4 sample only exhibited the adsorbed oxygen species and other oxygen impurities (Fig. 5B). In view of g-C_3N_4/MnO_2, a combined O 1s spectrum was obtained (Fig. 5B) with the binding energy of the lattice oxygen shifted to 529.3 eV. The N 1s spectrum of g-C_3N_4 (Fig. 5C) can be divided into three main peaks at 398.2, 399.7, and 401.2 eV, which can be assigned to the sp^2-hybridized nitrogen (C═N–C), bridging nitrogen ($(C)_3$–N), and N–H bonding in the g-C_3N_4 framework, respectively. When compared with the MnO_2 nanosheets, the N 1s binding energy of the C═N–C bond displayed a minor shift to higher value (Fig. 5D). These results suggested the formation of a Z-scheme system through the coating of MnO_2 onto the g-C_3N_4 nanosheets with electrons flowing from g-C_3N_4 to MnO_2 and achieving thermodynamic equilibrium. The XPS valence band spectra are also used for calculating band edge potentials, which can further explain the Z-scheme mechanism.[138]

3.4. SPV techniques

Recently, the SPV strategy has provided some new opportunities to study the charge transfer path of Z-scheme systems.[139] Typically, Kelvin probe force microscopy (KPFM) can easily obtain the photocatalysts' surface potential distribution with high spatial resolution and potential sensitivity.[140–143] Therefore, using KPFM-based SPV techniques to study the carrier transfer path of Z-scheme systems is an efficient technology. Guan and co-workers[144] reported a g-C_3N_4-based Z-scheme system through encapsulation of g-C_3N_4 into hollow In_2O_3 tubules. To gain a deeper understanding of the charge migration route, KPFM was proposed (Fig. 6A–D). Under dark conditions, the difference in potential between the sample surface and substrate surface was 51.87 mV. Conversely, under visible light illumination, the surface potential of the whole area is greatly reduced, suggesting the concentration of photogenerated e^- and h^+. Meanwhile, the difference in potential between the sample surface and substrate surface were decreased to 50.57 mV. This change confirmed that the photogenerated e^- migrated from the surface of g-C_3N_4 to the interior of In_2O_3, further illustrating the Z-scheme mechanism. Therefore, the SPV strategy is also very promising for the confirmation of the Z-scheme mechanism.

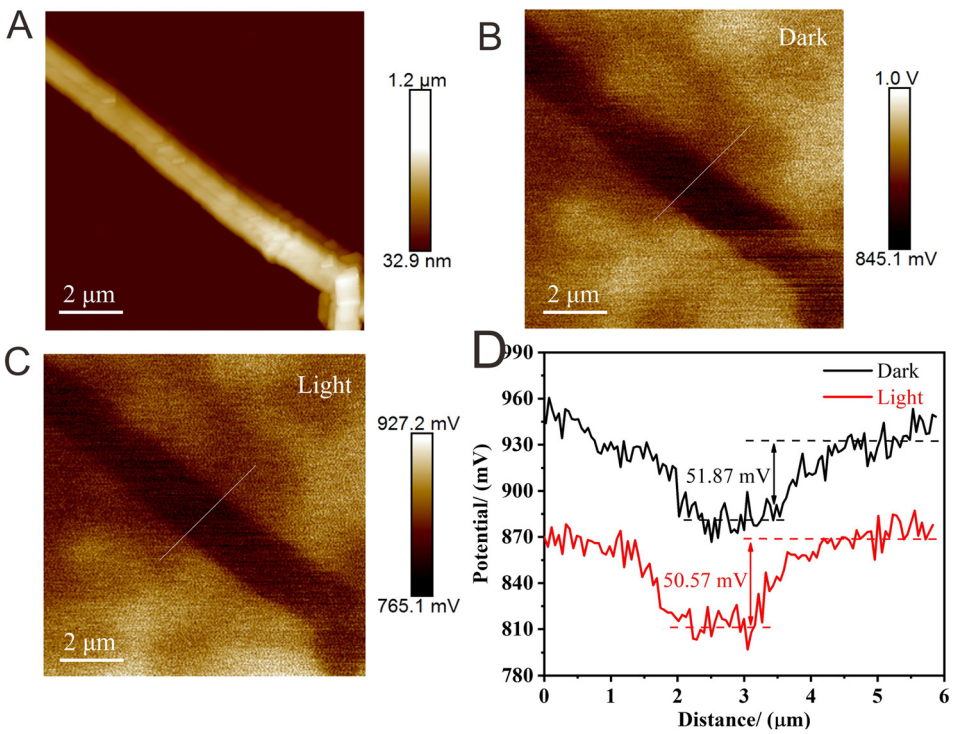

Fig. 6 (A) Atomic force microscopy image of the samples. (B) KPFM potential image of the samples under dark conditions. (C) KPFM potential image of the samples under light illumination. (D) The corresponding surface curves correspond to the white light. Reproduced with permission from ref. 144.

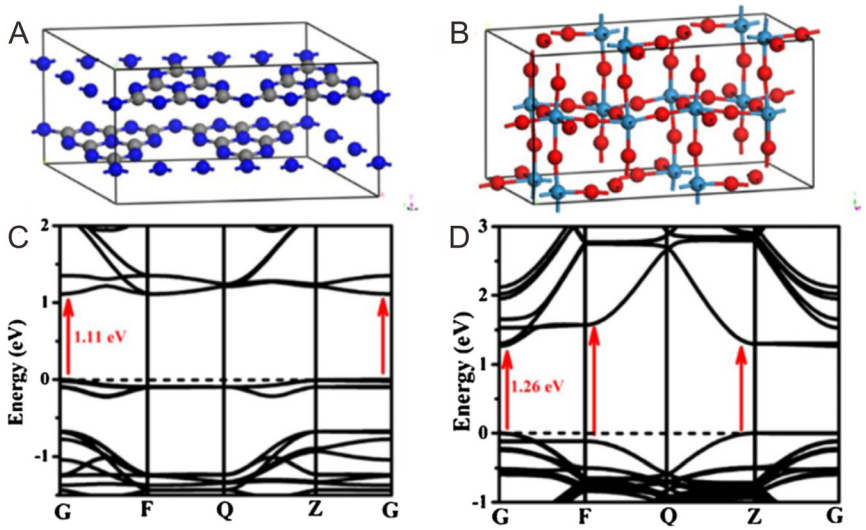

Fig. 7 Crystal structures of (A) g-C_3N_4 and (B) monoclinic WO_3. The calculated electronic band structures of (C) g-C_3N_4 and (D) WO_3. Reproduced with permission from ref. 127.

3.5. DFT calculation

It is well known that DFT calculation is a promising technology to explore the charge migration mechanism.[145,146] In detail, the first-principles simulation with a DFT calculation is commonly utilized for studying the charge transfer through analyzing the effective mass of its charge to estimate the recombination efficiency of the photogenerated carrier.[108,127,147] The DFT calculation is conducted based on the crystal and electronic band structures (Fig. 7).[127] The effective masses of the charges of WO_3 and g-C_3N_4 can be calculated through the parabolic fitting of their CB minimum and VB maximum based on eqn (1) and (2), respectively, and the separation efficiency of the photogenerated h^+ to the e^- based on eqn (3):

$$m^* = \hbar^2(d^2E/dk^2)^{-1} \quad (1)$$

$$v = \hbar k/m^* \quad (2)$$

$$D = m_h^*/m_e^* \quad (3)$$

where $\hbar$, d^2E/dk^2, k, m^*, v, D, m_h^*, and m_e^* respectively signify the reduced Planck constant, the coefficient of the second-order term in a quadratic fit of $E(k)$ curves for the band edge, the wave vector, the effective mass of a charge, the transfer efficiency of a charge, separation efficiency of the photogenerated h^+ to the e^-, and the effective mass of photogenerated h^+ and e^-.

The calculated effective masses of photogenerated e^- and h^+ and the relevant separation efficiency in *G–Z* and *G–F* directions are summarized in Table 1. The smaller D value for g-C_3N_4 (D = 1.36) indicates its faster recombination efficiency. In contrast to g-C_3N_4, the excited electrons of WO_3 exhibit a higher transfer efficiency from bulk to interface, and then transfer into g-C_3N_4. In this way, the interfacial electron transfer path in g-C_3N_4/WO_3 occurs from WO_3 to g-C_3N_4, which follows the direct Z-scheme mechanism.[127]

Table 1 Calculated effective masses of the charges of g-C_3N_4 and WO_3

Species	Effective mass	*G–F* direction	*G–Z* direction	*F–Q* direction	*Z–Q* direction
g-C_3N_4	m_h^*	0.72	71	—	—
	m_e^*	0.53	1.8	—	—
	D	1.36	39.44	—	—
WO_3	m_h^*	0.53	—	0.49	0.51
	m_e^*	0.16	—	0.17	0.14
	D	3.31	—	2.88	3.64

4. Preparation methods for g-C_3N_4-based Z-scheme photocatalysts

Until now, there have been a lot of approaches utilized for the preparation of g-C_3N_4-based Z-scheme photocatalysts, and selecting a suitable method is crucial. In the following sections, different preparation methods for g-C_3N_4-based Z-scheme photocatalysts are described. Their advantages and disadvantages are also discussed in Table 2.

4.1. Deposition–precipitation strategy

Deposition–precipitation strategy is regarded as an effective method for fabricating g-C_3N_4-based Z-scheme photocatalysts.[148] Narayanan and co-workers reported on a AgCl@g-C_3N_4 direct Z-scheme photocatalyst through a modified deposition-precipitation method.[149] $AgNO_3$ was firstly introduced into the g-C_3N_4 suspension, and then vigorously stirred to ensure full adsorption of Ag^+ on the g-C_3N_4 surface. Subsequently, the Cl^- ions and Ag^+ ions were fully coated on the g-C_3N_4 surface, and then reacted to form

Table 2 Comparison between different methods for the preparation of Z-scheme photocatalysts

Synthesis strategy	Merits	Demerits
Deposition–precipitation strategy	High-efficiency, simple, and low-cost	Uncontrollable morphology and easy aggregation
Hydrothermal and solvothermal strategy	(i) Facile, eco-friendly, and highly efficient (ii) Produced photocatalysts with a relatively high crystallinity, narrow size distribution, and controllable morphology	Complicated preparation process
Solid-state synthesis	High-efficiency, simple, and low-cost	Uncontrollable morphology and easy aggregation
Ion-exchange strategy	The formation of closely contact interface, and the initial morphology can be well preserved	Time- and cost-consuming and complicated preparation process
Electrospinning strategy	Very suitable for the preparation of 1D materials	Time- and cost-consuming, complicated preparation process, and low efficiency
Self-assembly strategy	Narrow size distribution and uniform morphology	Time- and cost-consuming, and complicated preparation process
Photo-deposition strategy	Facile, eco-friendly, and highly efficient	Easy aggregation
Mechanical agitation strategy	Facile, eco-friendly, and highly efficient, and reduced aggregation	Relatively poor interface contacts between the two semiconductors

the AgCl@g-C_3N_4 direct Z-scheme photocatalysts. The coating of AgCl on g-C_3N_4 was proved *via* XRD and FTIR spectra, which also confirmed the close interface between AgCl and g-C_3N_4 for greatly enhancing the photocatalytic performance.

4.2. Hydrothermal and solvothermal strategy

Hydrothermal and solvothermal approaches are usually conducted in a sealed autoclave under high temperature and pressure conditions, endowing the obtain semiconductors with high crystallinity, regulatable morphology, and homogeneous size distribution.[13,150–155] Therefore, this strategy is commonly utilized for fabricating g-C_3N_4-based Z-scheme photocatalysts without further post-treatment. Liu and co-workers[156] reported on Bi_2WO_6 quantum dots/g-C_3N_4 binary Z-scheme systems *via* a simple one-pot hydrothermal strategy. In this work, porous g-C_3N_4 ultrathin nanosheets provided a high specific surface area for decorating Bi_2WO_6 quantum dots, leading to a strong interaction between the Bi_2WO_6 quantum dots and g-C_3N_4 nanosheets.

4.3. Solid-state strategy

The solid-state strategy is commonly defined as the calcination of one precursor or multiple precursors in a gas atmosphere at an elevated temperature.[157,158] The homogeneous dispersion of the precursors plays an important role in affecting the quality and uniformity of the prepared materials. Several methods, such as intensive ball milling[159] and dissolving precursors in a solvent followed by drying,[160] can evidently stop the agglomeration of the precursors and maintain uniformity. The calcination parameters, such as heating rate and calcination temperature and time, can regulate the crystallinity, microstructure morphology, surface performance, and phase structure, which further affect the photocatalytic performance. Wang and co-workers[161] explored the effect of calcination temperature on the preparation of hierarchical TiO_2/g-C_3N_4 Z-scheme photocatalysts. The insertion of g-C_3N_4 nanoparticles on the porous TiO_2 framework was confirmed *via* SEM and XRD (Fig. 8A–G). The BET results indicated the effect of the calcination temperature on the porous structure (Fig. 8H and I). The specific surface area and pore volume gradually increased with increasing temperature to 550 °C, but a further increase in the temperature would lead to a reduction.

4.4. Ion exchange strategy

The ion exchange method mainly involves exchanging ions in an ionic crystal, but the framework still keeps close intact with each other.[162–164] Additionally, the ion exchange can be quickly accomplished when the temperature is raised. Wang and co-workers[165] prepared $Cd_xZn_{1-x}S$/Au/g-C_3N_4 Z-scheme photocatalysts through the ion exchange approach, which displayed improved photocatalytic H_2 production activity. Furthermore, when the ion exchange strategy is used, it is much easier to control the final product *via* adjusting the reaction conditions. Additionally, the Janus-like structures ensured them with improved visible light absorption and enlarged absorption range. Thus, the ion exchange method is an efficient approach for post-modification of Z-scheme systems.

4.5. Electrospinning strategy

It is well known that the electrospinning method is a versatile strategy to fabricate 1D materials, *e.g.*, nanofibers, nanotubes, nanobelts.[166,167] It can also be utilized for the preparation of 1D Z-scheme photocatalysts. A 1D nanostructure can boost the mobility of charge and enhance the absorption of visible light, and thus decrease the recombination of charge and enhance the photocatalytic performance.[168,169] Li and co-workers[170] prepared a TiO_2/g-C_3N_4/RGO ternary Z-scheme heterojunction *via* an electrospinning coupled approach. The crystal structure, morphology, composition, specific surface area,

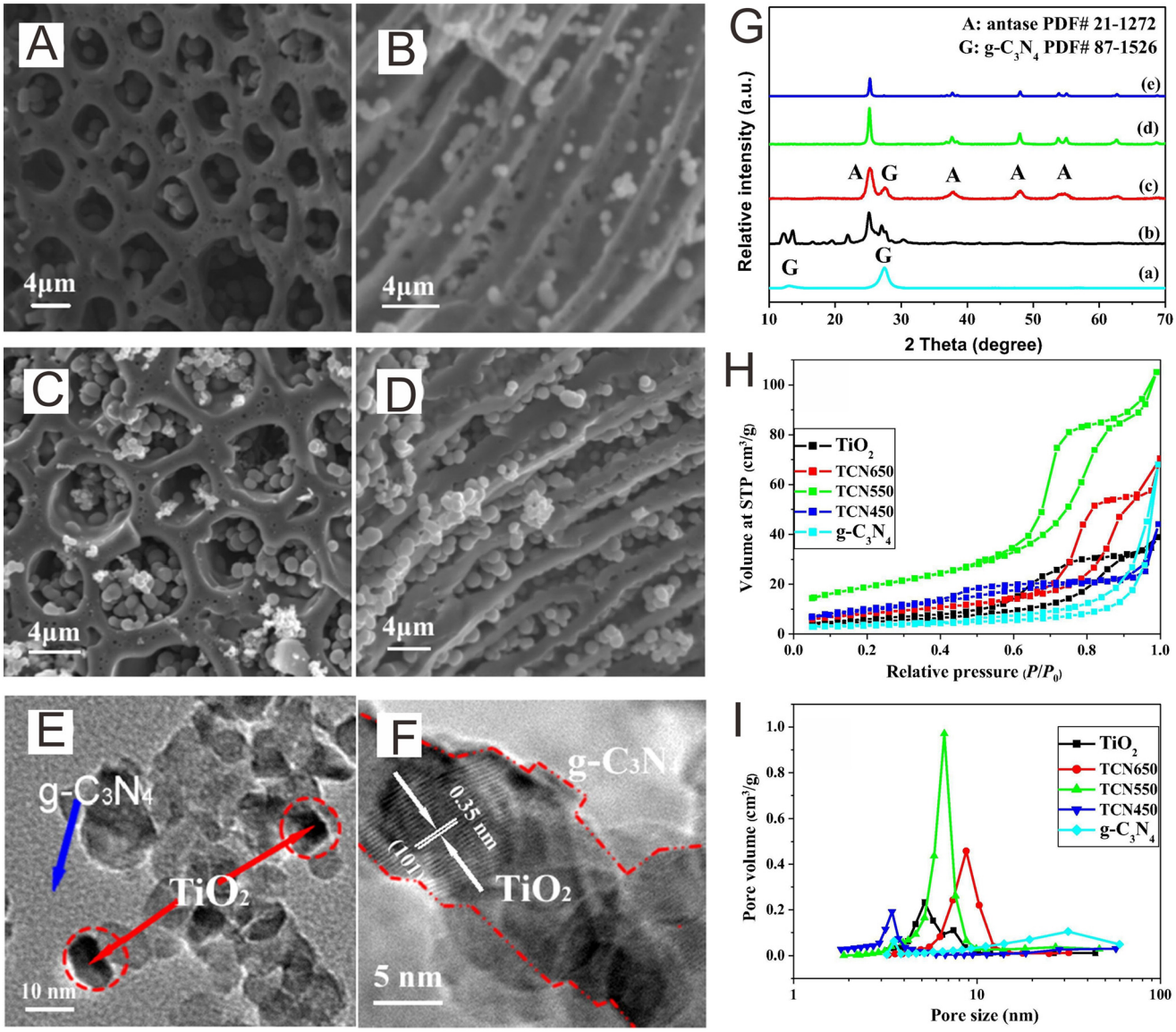

Fig. 8 SEM images at different perspective views of (A and B) the pure hierarchical TiO_2 framework and (C and D) the TiO_2/g-C_3N_4 Z-scheme photocatalyst calcination at 550 °C (denoted as TCN550). TEM (E) and HRTEM (F) images of the TCN550. XRD (G), N_2 adsorption isotherms (H), and pore size distribution (I) for the different samples. Reproduced with permission from ref. 161.

photoelectrochemical properties, and photocatalytic performance can be adjusted *via* electrospinning condition.

4.6. Self-assembly strategy

The self-assembly approach involves the spontaneous organization of a disordered component into an ordered structure and the optimization of the free energy.[8,171–174] Cheng and co-workers[175] proposed a simple electrostatic self-assembly approach for preparing g-C_3N_4/ZnO Z-scheme photocatalysts. In this system, the electrostatic force between g-C_3N and ZnO was very strong, which can concurrently enhance the charge separation and stability. When N-doped ZnO nanoplates were added to the exfoliated g-C_3N_4 suspension, the ZnO nanoplates' surface was spontaneously coated with g-C_3N_4 nanosheets to minimize the surface energy, resulting in the formation of a core–shell N-doped ZnO/g-C_3N_4 Z-scheme photocatalyst.[176] Therefore, the self-assembly method endows the Z-scheme photocatalysts with a narrow size distribution, regulatable morphology, and strong interaction.

4.7. Photo-deposition strategy

The photo-deposition method is the phenomenon in which a semiconductor is decorated on the other's surface *via* light illumination.[177–179] In this method, the CB potential of the semiconductor must be much lower than the reduction potential, and the VB potential must be higher than the oxidation potential.[129] The photo-deposition method is very

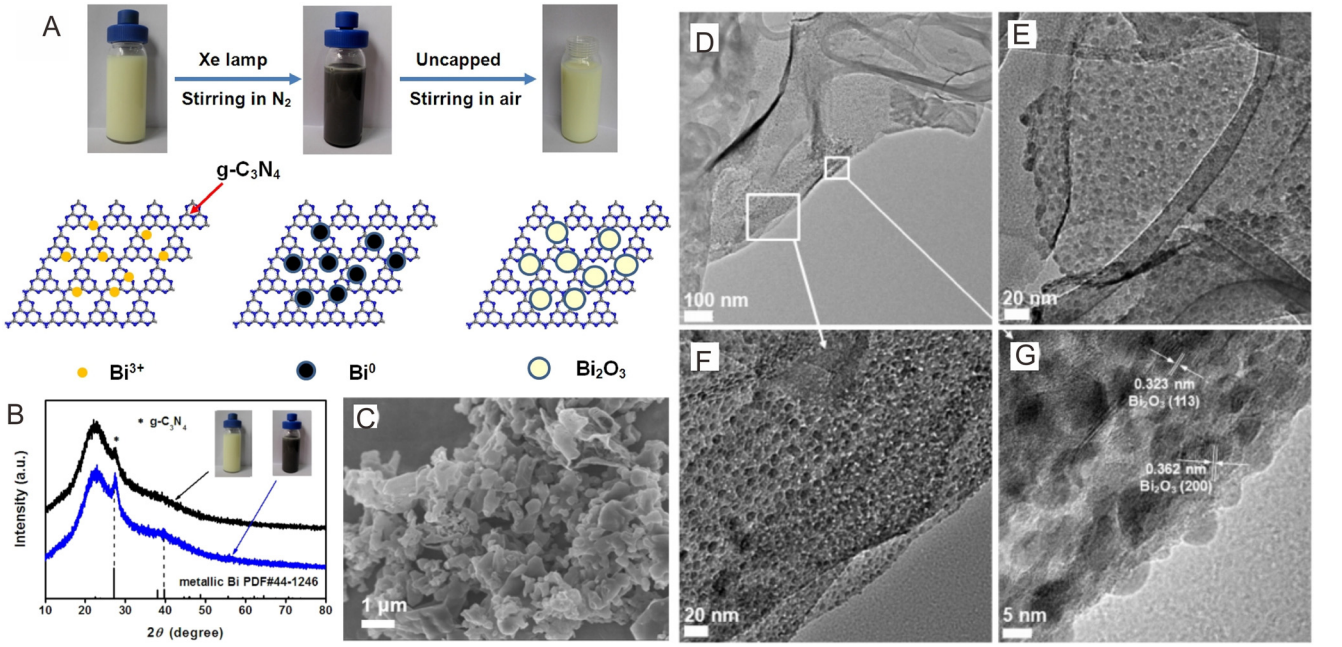

Fig. 9 (A) Diagrammatic sketch of the preparation of Bi_2O_3/g-C_3N_4. (B) XRD patterns of the intermediate products. (C) FESEM image of Bi_2O_3/g-C_3N_4. TEM (D–F) and HRTEM (G) images of Bi_2O_3/g-C_3N_4. Reproduced with permission from ref. 180.

promising for preparing Z-scheme photocatalysts. A Bi_2O_3/g-C_3N_4 direct Z-scheme photocatalyst was fabricated through the simple photoreductive deposition of Bi^{3+} on the g-C_3N_4 surface under light illumination, followed by air oxidation of Bi^{3+} to Bi_2O_3 (Fig. 9A).[180] The uniform dispersion of quantum-sized Bi_2O_3 on the g-C_3N_4 nanosheet surface could be observed from the XRD pattern, FESEM, TEM and HRTEM images (Fig. 9B–G). Wu and co-workers[181] reported a novel $BiVO_4$(040)–Ag@CdS Z-scheme photocatalyst in which Ag was selectively photo-deposited on the (040) facets of $BiVO_4$, and the CdS nanorods were decorated on $BiVO_4$(040)–Ag. Thus, the photo-deposition strategy is also a promising technology for decorating one semiconductor with the other semiconductor, which further improves the charge separation.

4.8. Mechanical agitation approach

The conventional mechanical agitation strategy involves the attachment of two pre-prepared semiconductors *via* physical methods, such as grinding,[182] impregnation,[183] planetary ball-milling,[184] and reflux.[185] However, the semiconductors assembled through these methods have no close interface, and they are easily separated from each other, resulting in a low charge transfer efficiency and moderate photocatalytic performance.[186] Ohno and coworkers[187] fabricated three kinds of g-C_3N_4/WO_3 Z-scheme photocatalysts *via* grinding, impregnation assisted with sonication, and planetary ball-milling methods. Different from the agglomerated WO_3 decorated on the g-C_3N_4 nanoplate prepared through the first two methods, WO_3 prepared through planetary ball-milling strategy was uniformly dispersed on the g-C_3N_4 nanoparticles, which was beneficial for improving the specific surface area and photocatalytic performance.

Among the various fabrication strategies, deposition–precipitation, hydrothermal and solvothermal, solid-state synthesis, ion-exchange, electrospinning, self-assembly, and photo-deposition strategies are beneficial for achieving a strong interaction and intimate interface between the two semiconductors, which will lead to improved charge migration efficiency.[76,188] The strong interaction (*e.g.*, covalent bond, ionic bond, and coordination bond) and wear interaction (hydrogen bond and van der Waals force) can be formed between the two semiconductors, serving as charge transfer channels and enhancing the interface contact. Especially, the ion-exchange strategy is very promising for forming a close contact interface, and the initial morphology can be retained.[189,190] The self-assembly method can ensure the two semiconductors with a narrow size distribution and uniform morphology.[191] In contrast, the mechanical agitation method exhibits relatively poor interface contact between the two semiconductors, resulting in low photocatalytic performance.[192] Nevertheless, this strategy is simple and cost effective, and shows great potential in practical production (Table 2).

5. Photocatalytic organic pollutant degradation

Many organic pollutants, such as methylene blue (MB), methyl orange (MO), 4-nitrophenol (4-NP), rhodamine B (RhB), basic fuchsin (BF), bisphenol A (BPA), brilliant blue (BB), 2,4-dichlorophenol (2,4-DCP), tetracycline (TC), sulfamethoxazole (SMX), indomethacin (IDM), and others

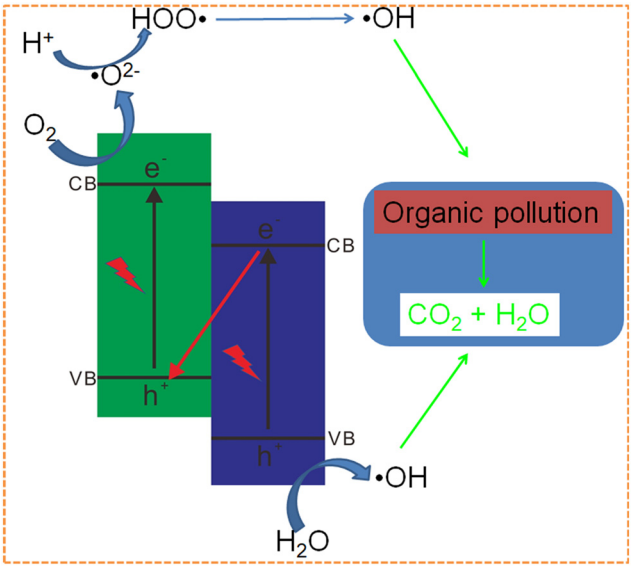

Fig. 10 Diagrammatic explanation of organic pollutant degradation over g-C_3N_4-based Z-scheme photocatalysts.

have recently been excessively discharged to soil and water, which have negative influences on the environment and human health.[193–201] g-C_3N_4-based Z-scheme photocatalysts have gained growing attention for organic pollutant removal because of their enhanced photocatalytic efficiency and stability (Fig. 10).[77,101,202] Some important examples for photocatalytic organic pollutant degradation are shown below, and their property comparison is shown in Table 3.

5.1. g-C_3N_4/TiO_2 Z-scheme photocatalysts

TiO_2 is valuable in the photocatalytic fields because of its unique advantages, *e.g.*, excellent controllability, large surface area, amazing stability, and ease of recycling.[203,204] Some investigations have focused on combining TiO_2 with g-C_3N_4 to develop Z-scheme photocatalysts for achieving better photocatalytic property. The first example was reported by Yu and co-workers,[73] who achieved markedly enhanced photocatalytic properties by g-C_3N_4/TiO_2 Z-scheme photocatalysts. Dong and co-workers[205] fabricated an all-solid-state (ASS) Z-scheme photocatalyst through decorating g-C_3N_4 nanosheets on TiO_2 nanotube arrays (TNTAs). The as-prepared photocatalyst displayed improved photocatalytic property for RhB degradation, which was about 4 times greater than that exhibited by pure TiO_2 TNTAs. Ho and co-workers[206] prepared the g-C_3N_4 quantum dots (QDs)-modified rutile TiO_2 (rTiO_2) (g-C_3N_4 QDs-rTiO_2) hybrid *via* calcination of the mixture of P25 TiO_2 and melamine under 500 °C for 4 h, which displayed excellent photocatalytic properties for the RhB degradation. Facet engineering is crucial for improving the photocatalytic performance. The exposed {010} and {110} crystal facets of $BiVO_4$ have been demonstrated to be the active reduction and oxidation sites, respectively.[207] Raj and co-workers[208] fabricated a g-C_3N_4/TiO_2/CuO Z-scheme heterostructure *via* a simple hydrothermal strategy, which displayed improved photocatalytic performance of (90.3%) RhB dye degradation within 120 min. In addition, almost no loss in photocatalytic activity after 5 cycles was found. The Lv group[209] studied the influence of the exposed {001} and {101} facets of TiO_2 on the photocatalytic activity. They first fabricated TiO_2 nanosheets (NSs) and TiO_2 nanoboxes (NBs), and then combined them with g-C_3N_4 to prepare TiO_2 NS/g-C_3N_4 and TiO_2 NBs/g-C_3N_4, respectively (Fig. 11A and B). The {001} facets of TiO_2 NSs came into contact with g-C_3N_4 (Fig. 11A and C), and the {101} facets of TiO_2 NBs came into contact with g-C_3N_4 (Fig. 11B and D). Under visible light illumination, the photogenerated carriers on TiO_2 were separately accumulated on the {101} and {001} facets.[210] The photogenerated electrons were subsequently centered on the {101} facets of the TiO_2 NBs, which could transfer to g-C_3N_4 for photocatalytic reactions, which is in line with the direct Z-scheme mechanism (Fig. 11F). Thus, the e^-–h^+ separation efficiency of TiO_2 NBs/g-C_3N_4 is much higher than that of TiO_2 NSs/g-C_3N_4, and the TiO_2 NBs/g-C_3N_4 displayed the highest photocatalytic efficiency (Fig. 11E). This work offers us a new design concept, wherein the suitable interface engineering of the exposed facets of a pure semiconductor in a direct Z-scheme photocatalyst is able to effectively enhance the e^-–h^+ separation, which can further improve the photocatalytic property.

5.2. g-C_3N_4/WO_3 Z-scheme photocatalysts

WO_3 is gradually becoming recognized as one of the most promising photocatalysts, owing to its outstanding photocatalytic performance, chemical inertness, and optical stability.[211,212] In comparison with TiO_2, WO_3 possesses a smaller band gap (2.7 eV) and more positive CB level. Thus, it is also favorable for combining with g-C_3N_4 to construct Z-scheme photocatalysts. The Chen group[213] developed a WO_3/g-C_3N_4 Z-scheme photocatalyst. The reaction rate constants for degrading MB and BF over WO_3(5.0 wt%)/g-C_3N_4 were found to be 4.77 and 3.84 times greater than that of the bare g-C_3N_4, respectively. The Jia group[214] developed a new bifunctional WO_3/g-C_3N_4 Z-scheme photocatalyst by *in situ* liquid phase strategy. The photocatalytic degradation efficiency of the 30 wt%WO_3/g-C_3N_4 was found to be 2.5 and 2.7 times higher than the individual g-C_3N_4 and WO_3, respectively. Kang and co-workers[215] fabricated WO_3/g-C_3N_4 Z-scheme photocatalysts through a simple one-step simultaneous heating approach utilizing urea as the starting material, which exhibited markedly improved photocatalytic property for MB degradation. Chai and co-workers[216] constructed a WO_3/g-C_3N_4 Z-scheme photocatalyst through *in situ* acidic precipitation and subsequent calcination processes, which also showed improved photocatalytic property for RhB degradation. Zheng and co-workers[217] reported a C-doped g-C_3N_4/WO_3 Z-scheme photocatalyst through the hydrothermal strategy. Benefiting from high specific areas, C-substitution, and Z-scheme mechanism, the

Table 3 Comparison of the photocatalytic organic pollution degradation performance over g-C_3N_4-based Z-scheme photocatalysts

Photocatalysts	Preparation strategy	Mass (mg)	Light source	Target pollutant/initial concentration	Degradation time (min) and rate (%)	K_{app}[a] [10^{-2} min^{-1}]	Ref.
g-C_3N_4/TiO_2	Calcination route	300	15 W UV lamp, 365 nm	HCHO/170 ppm	60 (~94)	7.36	73
g-C_3N_4/TiO_2	Electrochemical route	—	300 W xenon lamp, >420 nm	RhB/5 mg L^{-1}	300 (~77)	4.48	205
g-C_3N_4/rTiO_2	Calcination route	50	500 W xenon lamp, >420 nm	RhB/5 mg L^{-1}	240 (~98)	11.5	206
g-C_3N_4/TiO_2/CuO	Hydrothermal strategy	50	500 W xenon lamp	RhB/0.5 mg L^{-1}	120 (~97)	0.95	208
g-C_3N_4/TiO_2-HNB	Microwave-assisted strategy	—	3 W LED lamp, 365 nm	Brilliant red X-3B/1.0 × 10^{-4} mmol L^{-1}	45 (~99)	5.1	209
WO_3/g-C_3N_4	Ball milling and heat treatment methods	10	500 W xenon lamp, >470 nm	MB and BF/0.9 × 10^{-5} and 1.0 × 10^{-5} mol L^{-1}	MB 120 (~99) BF 120 (~97)	—	213
WO_3/g-C_3N_4	*In situ* liquid phase process	50	300 W xenon lamp, >400 nm	MB/50 mg L^{-1}	90 (~97)	1.90	214
WO_3/g-C_3N_4	One-step heating procedure	30	500 W xenon lamp, >420 nm	RhB/5 mg L^{-1}	120 (~90)	—	215
C-doped g-C_3N_4/WO_3	Cellulose-assisted strategy	100	500 W xenon lamp, >420 nm	TC/10 mg L^{-1}	60 (~70)	—	217
WO_3/g-C_3N_4/Bi_2O_3	One step co-calcination way	100	300 W xenon lamp, >420 nm	TC/10 mg L^{-1}	60 (~80)	2.37	159
g-C_3N_4/MnO_2	Wet-chemical method	50	300 W xenon lamp	RhB/10 mg L^{-1}	180 (~77)	3.3	137
Bi_2O_3/g-C_3N_4	Ball milling and heat treatment methods	5	500 W xenon lamp, 470 nm	MB and RhB/1.1 × 10^{-5} and 1.0 × 10^{-5} mol L^{-1}	MB 120 (~76) RhB 120 (~73)	2.53 and 1.01	223
g-C_3N_4/Bi_2O_3/$BiPO_4$	Calcination route	15	—	MO/10 mg L^{-1}	160 (~88)	1.15	225
β-Bi_2O_3/g-C_3N_4	Hydrothermal calcination approach	40	350 W xenon lamp, >420 nm	RhB/1 × 10^{-5} mol/L	80 (~97)	4.22	226
g-C_3N_4/Bi_4O_7	Calcination method	80	500 W halogen lamp, 420–800 nm	MB and RhB/— and —	90 (~80)	1.73	227
g-C_3N_4/Bi_2WO_6	Mixing and heating method	50	300 W xenon lamp, 350–780 nm	2,4-DCP/20 mg L^{-1}	120 (>99)	1.13	228
g-C_3N_4/Bi_2WO_6	One-pot hydrothermal strategy	50	Xenon lamp (XL-300, Yirda)	RhB/10 mg L^{-1}	30 (>99)	8.17	156
g-C_3N_4/RGO/Bi_2WO_6	Hydrothermal method	250	500 W xenon lamp, >420 nm	TCP/20–100 mg L^{-1}	120 (>99)	3.15	229
Ag-decorated g-C_3N_4/Bi_2WO_6	Polymerization method	40	300 W xenon lamp, 400 nm	RhB/10 mg L^{-1}	90 (>99)	—	230
Bi_3O_4Cl/g-C_3N_4	Solid-phase calcination method	50	250 W xenon lamp, >420 nm	RhB and TC/10 and 10 mg L^{-1}	RhB 60 (>98) TC 60 (>76)	— and 2.05	231
BiOBr/RGO/pg-C_3N_4	Solvothermal method	50	300 W xenon lamp, 420 nm	RhB and TC/10 and 10 mg L^{-1}	RhB 7.5 (>99) TC 60 (>97)	— and —	232
$Bi_{12}GeO_{20}$/g-C_3N_4	Sol–gel method	300	300 W Dy lamp, 400 nm	RhB/5 mg L^{-1}	50 (>99)	2.55	233
g-C_3N_4/C@Bi_2MoO_6	Hydrothermal deposition method	100	500 W xenon lamp, >420 nm	β-Naphthol/15 mg L^{-1}	150 (>62)	0.63	234
Ag_3PO_4/g-C_3N_4	*In situ* precipitation method	5	300 W xenon lamp, >400 nm	SMX/1 mg L^{-1}	10 (~98)	6.3	238
Ag_3PO_4/g-C_3N_4	*In situ* precipitation method	30	300 W xenon lamp	MO/10 mg L^{-1}	5 (>99)	—	239
g-C_3N_4/Ag_2WO	*In situ* precipitation method	30	300 W xenon lamp	MO/10 mg L^{-1}	150 (~98)	—	240
Ag_2CrO_4/g-C_3N_4	Precipitation method	20	300 W xenon lamp, >400 nm	MO and RhB/10 and 10 mg L^{-1}	MO 21 (~90) RhB 40 (~97)	9.64 and 9.21	241
Ag@AgBr/g-C_3N_4	Deposition–precipitation method	100	300 W xenon lamp	MO and MB/10 and 10 mg L^{-1}	MO 10 (~97) RhB 10 (~96)	— and —	117
Ag_2CrO_4/Ag/g-C_3N_4	*In situ* growth and photoreduction methods	50	500 W xenon lamp, <420 nm	2,4-DCP/10 mg L^{-1}	120 (~96)	1.52	243
g-C_3N_4/Ag/MoS_2	*In situ* growth and precipitation methods	100	300 W xenon lamp, >420 nm	RhB/20 mg L^{-1}	60 (>99)	—	247
g-C_3N_4/ZnO	Ultrasonically exfoliated method	100	300 W xenon lamp, >420 nm	4-CP/10^{-4} mol L^{-1}	90 (>99)	5.09	248
CdS/RGO/g-C_3N_4	Hydrothermal method	20	350 W xenon lamp	Atrazine/—	300 (~92)	0.71	249
g-C_3N_4–RGO–TiO_2	Liquid-precipitation strategy	50	300 W xenon lamp, >420 nm	RhB/30 mg L^{-1}	180 (~92)	1.37	250
MoO_3/g-C_3N_4	Calcination method	30	350 W xenon lamp, >420 nm	TC/20 mg L^{-1}	90 (~90)	2.23	251
p-type Cu_3P/n-type g-C_3N_4	Calcination method	10	300 W xenon lamp, 400 nm	RhB/—	20 (>99)	—	252

Table 3 *(continued)*

Photocatalysts	Preparation strategy	Mass (mg)	Light source	Target pollutant/initial concentration	Degradation time (min) and rate (%)	K_{app}[a] [10^{-2} min^{-1}]	Ref.
$NiTiO_3$/g-C_3N_4	Calcination method	40	30 W visible LED	RhB/10 mg L^{-1}	—	3.09	253
$LaFeO_3$/g-C_3N_4	Calcination method	30	300 W xenon lamp, >420 nm	RhB/25 mg L^{-1}	60 (~98)	6.22	120
V_2O_5/g-C_3N_4	*In situ* growth strategy	50	250 W xenon lamp, 420 nm	RhB and TC/10 and 10 mg L^{-1}	120 (~77)	4.91 and —	107
SnO_{2x}/g-C_3N_4	Calcination method	100	350 W xenon lamp, >420 nm	RhB/10 mg L^{-1}	40 (>99)	1	254
$InVO_4$/Bi_2S_3/g-C_3N_4	Wet-impregnation method	200	300 W xenon lamp, >420 nm	RhB19/15 mg L^{-1}	100 (~96)	0.57	255
CDs/g-C_3N_4/SnO_2	Thermal polymerization	10	300 W xenon lamp, >420 nm	IDM/10 mg L^{-1}	40 (>99)	2.33	256
g-C_3N_4/$ZnFe_2O_4$/UiO-66	Hydrothermal method	—	300 W xenon lamp, >420 nm	RhB/—	40 (>99)	4.89	256
g-C_3N_4/$BiVO_4$/$CoFe_2O_4$	High-temperature solid-state route	50	300 W xenon lamp, >400 nm	RhB/—	25 (>99)	2.84	257
g-C_3N_4/g-C_3N_4	Bottom-up approach	10	50 W xenon lamp, >400 nm	RhB/10 mg L^{-1}	240 (>99)	1.39	246

[a] K_{app} represents the reaction rate constant.

prepared Z-scheme photocatalysts displayed a narrow bandgap, and improved visible-light absorption and separation efficiency of charge. All of the abovementioned improved photocatalytic properties of the WO_3/g-C_3N_4 composites were mainly because of the unusual merits of the Z-scheme photocatalytic systems.

5.3. g-C_3N_4/MnO_2 Z-scheme photocatalysts

MnO_2 is gradually becoming recognized as an efficient photocatalyst owing to its excellent photocatalytic performance, suitable bandgap value, and optical stability.[218] Xu and co-workers[137] prepared g-C_3N_4/MnO_2 Z-scheme photocatalysts. There were many functional groups and exposed lone pair electrons from N atoms on the g-C_3N_4 surfaces, which provided abundant adsorption sites for Mn^{2+} ions (Fig. 12A). It should be noted that the thicknesses of the g-C_3N_4 nanosheets, MnO_2 nanosheets, and the g-C_3N_4/MnO_2 hybrid were approximately 3.4, 2.2, and 5.7 nm, respectively, which were roughly equal to the stacking distance of the g-C_3N_4 and MnO_2 nanosheets (Fig. 12B–D). The electrostatic potentials of MnO_2 (001) and g-C_3N_4 (001) were measured to be 6.8 and 4.5 eV, respectively, suggesting that the electrons on the g-C_3N_4 will spill onto MnO_2 *via* the interface (Fig. 12E–G).[219,220] Thus, g-C_3N_4 was more positively charged. Photocatalytic experiments suggested that the prepared g-C_3N_4/MnO_2 exhibited better photocatalytic property when compared with the bare g-C_3N_4 and MnO_2 (Fig. 12H and I). Herein, electronic paramagnetic resonance (EPR) analysis can be used to survey the reactive species. The results indicated that the transfer of the photogenerated carrier in g-C_3N_4/MnO_2 should obey the direct Z-scheme mechanism (Fig. 12J and K). Moreover, the positive slopes of the Mott–Schottky plots indicated that both g-C_3N_4 and MnO_2 are typical n-type semiconductors (Fig. 12J and K). With regard to n-type semiconductors, the flat-band potential is nearly that same as that for CB,[221,222] and the CB of g-C_3N_4 and MnO_2 were measured to be −1.61 and 1.22 V, respectively (Fig. 12L and N). The VB positions were calculated by XPS spectroscopy (Fig. 12M), and the results showed that the VB of g-C_3N_4 and MnO_2 were about 1.81 and 3.26 V, respectively. Therefore, a Z-scheme transfer mechanism can be used to illustrate the enhanced photocatalytic property over the g-C_3N_4/MnO_2 hybrids. As for the individual g-C_3N_4 or MnO_2, the photogenerated h^+ in g-C_3N_4 cannot oxidize OH^- to produce $^{\bullet}OH$ radicals and the photogenerated e^- in MnO_2 cannot generate $^{\bullet}O^{2-}$ radicals, respectively, because of the thermodynamic equilibrium limit. After the Z-scheme heterojunction was formed, the photogenerated e^- in the CB of MnO_2 will migrate to the VB of g-C_3N_4 and then combine with the h^+. The Z-scheme configuration can explain the enhanced photocatalytic property well (Fig. 13O).

5.4. g-C_3N_4/bismuth oxide Z-scheme photocatalysts

Recently, multifarious bismuth-based semiconductors, *e.g.*, Bi_2O_3,[159,180,223–225] β-Bi_2O_3,[226] Bi_4O_7,[227] Bi_2WO_6,[156,228–230] Bi_3O_4Cl,[231] BiOBr,[232] $Bi_{12}GeO_2$,[233] Bi_2MoO_6,[234] have been reported for combining with g-C_3N_4 to form Z-scheme photocatalysts because of their unique characteristics, such as outstanding electrical property, appropriate energy band positions, and highly efficient photocatalytic performance.[235–237] For example, Chen and co-workers[223] prepared a Z-scheme Bi_2O_3/g-C_3N_4 photocatalyst. The reaction rate constants of Bi_2O_3 (1.0 wt%)/g-C_3N_4 for MB and RhB degradation were approximately 3.4 and 5 times greater that of the bare g-C_3N_4 and Bi_2O_3, respectively. The Z-scheme mechanism was confirmed through various technologies (*e.g.*, ESR, PL-TA and PL, *etc.*), which resulted in enhanced photocatalytic property. Du and co-workers[227] fabricated a

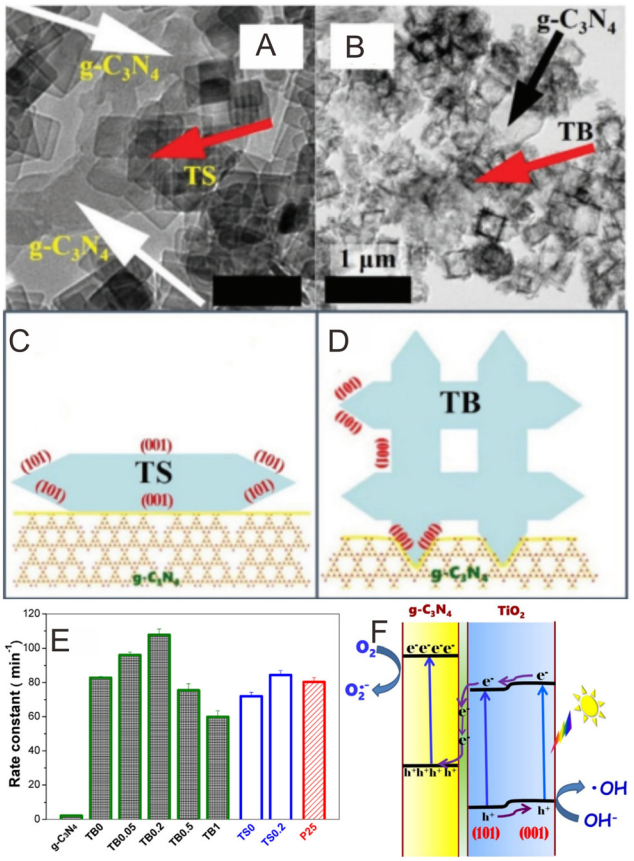

Fig. 11 TEM images of (A) TiO_2 NSs/g-C_3N_4 and (B) TiO_2 NBs/g-C_3N_4. Diagrammatic sketch of the contact interface between TiO_2 and g-C_3N_4 on (C) TiO_2 NSs/g-C_3N_4 and (D) TiO_2 NBs/g-C_3N_4. (E) Comparison of the photocatalytic activity of the synthesized photocatalysts for the photocatalytic degradation of brilliant red X3B. (F) Diagrammatic sketch for the photoinduced charge carrier migration mechanism in the TiO_2/g-C_3N_4 hybrids. Reproduced with permission from ref. 209.

high-performance g-C_3N_4/Bi_4O_7 Z-scheme photocatalyst *via* a simple way. In contrast to the single photocatalysts, the as-prepared g-C_3N_4/Bi_4O_7 photocatalyst displayed enhanced degradation efficiency toward MB, phenol, RhB, and BPA. The improved photocatalytic performance should be attributed to the improved light utilization and the highly efficient Z-scheme charge migration. Zhao and co-workers[228] reported a simple mixing and heating strategy to fabricate the g-C_3N_4/Bi_2WO_6 Z-scheme photocatalyst. The optimal dechlorination rate constant of 2,4-DCP over g-C_3N_4/Bi_2WO_6 was 1.13 h^{-1}, exceeding those of the bare g-C_3N_4 and Bi2WO_6 by 7.6 and 8.9 times, respectively. Yin and co-workers[233] prepared a new ASS $Bi_{12}GeO_{20}$/g-C_3N_4 Z-scheme photocatalyst. The obtained $Bi_{12}GeO_{20}$/g-C_3N_4 photocatalyst displayed improved photocatalytic property for degrading microcystin-LR and RhB in contrast to the individual $Bi_{12}GeO_{20}$ and g-C_3N_4. The enhanced photocatalytic property is because of the enhanced light utilization efficiency and effective spatial separation of the photo-generated carriers. In short, bismuth-based semiconductors can couple well with g-C_3N_4 to fabricate Z-scheme photocatalysts for enhancing photocatalytic properties owing to their suitable CB and CB values.

5.5. g-C_3N_4/Ag-containing semiconductor Z-scheme photocatalysts

Ag-containing photocatalysts can greatly improve the photocatalytic property of g-C_3N_4 through the Z-scheme mechanism. Some examples of Ag-containing photocatalysts with improved properties include Ag_3PO_4/g-C_3N_4,[238,239] Ag_2WO_4/g-C_3N_4,[240] and Ag_2CrO_4/g-C_3N_4.[241] In particular, utilizing noble metal Ag as the electron mediator for fabrication of Ag-containing semiconductors/g-C_3N_4 SCS Z-scheme photocatalysts can achieve more effective photocatalytic performance.[242] The Guo group[117] fabricated various Ag@AgBr/g-C_3N_4 Z-scheme photocatalysts *via* the photoreduction of AgBr/g-C_3N_4 hybrids. A dramatically improved photocatalytic property of Ag@AgBr/g-C_3N_4 was achieved, and is mainly attributed to the high light utilization and Z-scheme mechanism. Quan and co-workers[243] prepared Ag_2CrO_4/Ag/g-C_3N_4 Z-scheme photocatalysts *via* simple *in situ* growth and photoreduction strategies. Because of the strong light utilization, effective separation of the photogenerated e^- and h^+, and the excellent redox ability, the obtained Ag_2CrO_4/Ag/g-C_3N_4 hybrids showed remarkably improved photocatalytic performance for 2,4-DCP degradation, exceeding that of the pure g-C_3N_4 by 5.2 times.

5.6. Metal-free g-C_3N_4-based Z-scheme photocatalysts

Fabricating metal-free g-C_3N_4-based Z-scheme photocatalysts is a very promising and environmentally friendly method for degrading organic pollutants.[244,245] Huang and co-workers[246] constructed a metal-free 2D g-C_3N_4/g-C_3N_4 Z-scheme photocatalyst *via* utilization of a bottom-up approach. Profiting from the 2D morphology with the large exposed active site and the Z-scheme mechanism with the efficient separation of the photoinduced carriers, the fabricated 2D g-C_3N_4/g-C_3N_4 Z-scheme photocatalysts showed better photocatalytic performance when compared to the conventional g-C_3N_4/g-C_3N_4 homojunction and bulk g-C_3N_4. This work provides some new design concepts for Z-scheme systems with specific 2D morphology for enhanced organic pollutant removal.

5.7. g-C_3N_4-based SCS Z-scheme photocatalysts

As mentioned above, the g-C_3N_4-based SCS Z-scheme photocatalysts seem to be more promising for organic pollutant degradation. Among them, conductors acting as intermediates are utilized to link two semiconductors for the more favorable migration of the photogenerated carriers.[33] A typical example was presented by the Fang group.[247] They prepared a Z-scheme g-C_3N_4/Ag/MoS_2 ternary plasmonic Z-scheme photocatalyst with flowerlike nanostructures with a diameter of ~0.4–0.6 μm (Fig. 13A). The prepared g-C_3N_4/Ag/MoS_2 showed

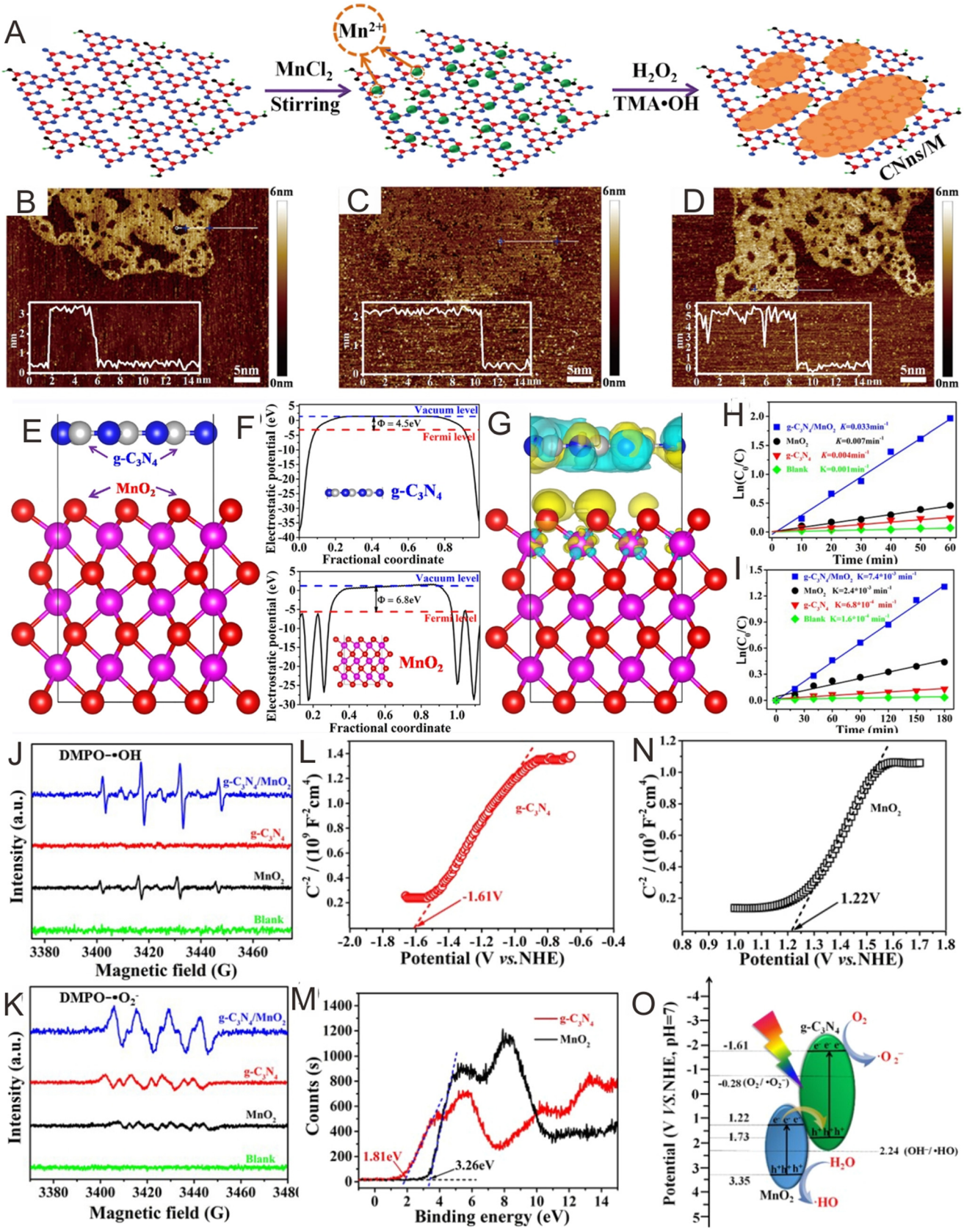

Fig. 12 (A) Diagrammatic sketch of g-C_3N_4/MnO_2 prepared through *in situ* growth of MnO_2 on the g-C_3N_4 nanosheets. AFM images of the (B) g-C_3N_4 nanosheets, (C) MnO_2 nanosheets, and (D) g-C_3N_4/MnO_2. (E) Optimized structure model of g-C_3N_4/MnO_2. (F) Calculated electrostatic potentials for g-C_3N_4 and the MnO_2 nanosheets, respectively. (G) Charge density difference model of g-C_3N_4/MnO_2. Photocatalytic degradation efficiency of (H) RhB and (I) phenol over g-C_3N_4, MnO_2, and g-C_3N_4/MnO_2 under light irradiation. (J) EPR spectra of DMPO–•OH through irradiation for 120 s in an aqueous dispersion and (K) DMPO–•O^{2-} through irradiation for 120 s in a methanol dispersion in the existence of g-C_3N_4, MnO_2, and g-C_3N_4/MnO_2. Mott–Schottky plots for (L) g-C_3N_4 and (M) MnO_2 nanosheets. (N) XPS valence band spectra of MnO_2 and g-C_3N_4 nanosheets. (O) Photocatalytic mechanism of g-C_3N_4/MnO_2. Reproduced with permission from ref. 137.

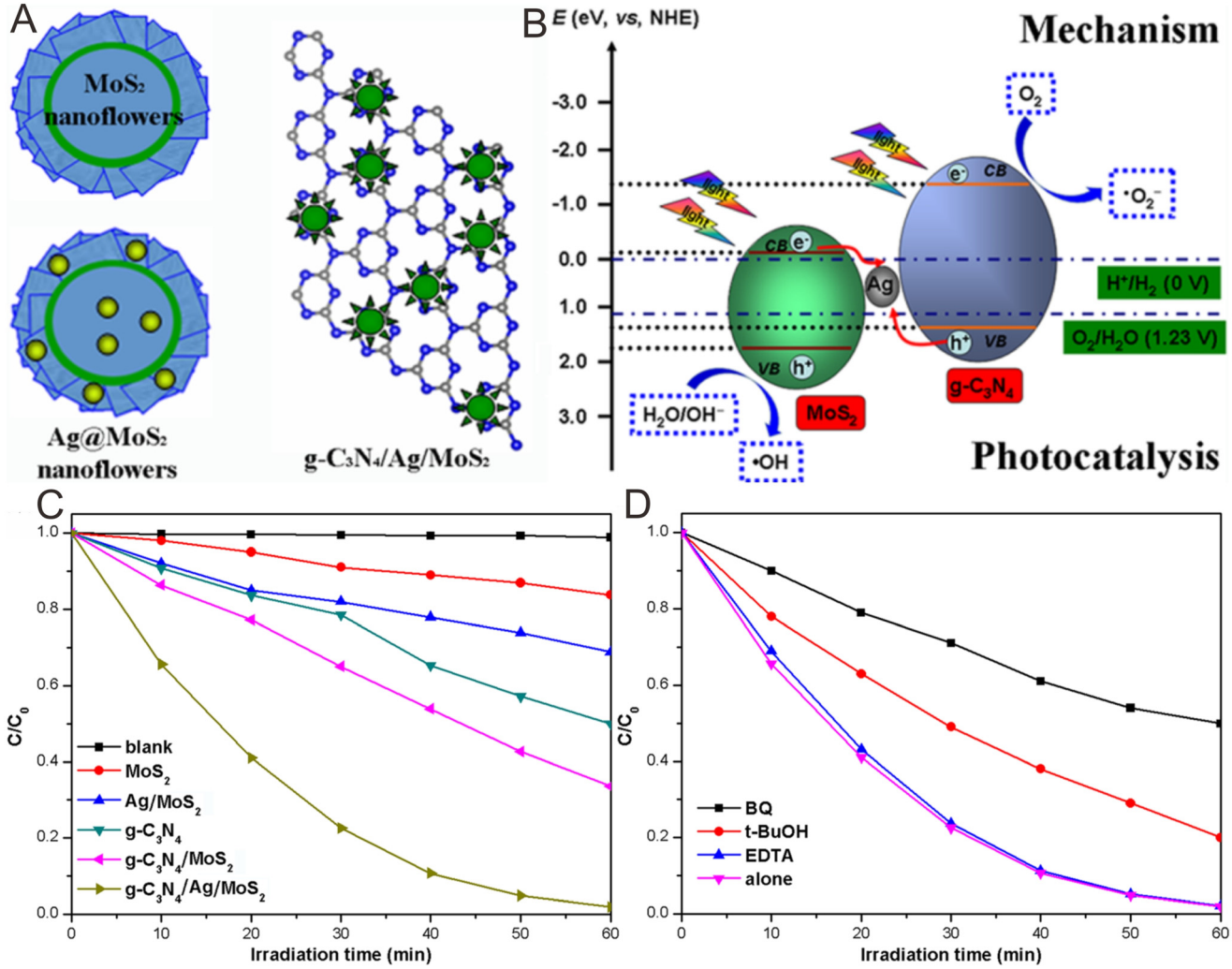

Fig. 13 (A) The nanostructures of Ag/MoS_2 and $g\text{-}C_3N_4/Ag/MoS_2$. (B) Diagrammatic sketch for the separation and migration of the photogenerated charges over $g\text{-}C_3N_4/Ag/MoS_2$. (C and D) Photocatalytic property of the fabricated MoS_2, Ag/MoS_2, $g\text{-}C_3N_4$, $g\text{-}C_3N_4/MoS_2$, and $g\text{-}C_3N_4/Ag/MoS_2$ photocatalysts for RhB solution. Reproduced with permission from ref. 247.

significantly enhanced photocatalytic performance, exceeding that of the Ag/MoS_2 and $g\text{-}C_3N_4/MoS_2$ systems by 9.43 and 3.56 times, respectively (Fig. 13C and D). The excellent photocatalytic property was mainly because of the synergetic effects of the Ag, $g\text{-}C_3N_4$, and MoS_2 nanophase structures, which led to a Z-scheme-mechanism-induced rapid separation of the photogenerated e^-–h^+ pairs and further enhanced photocatalytic property (Fig. 13B).

5.8. Others

In addition to the above common $g\text{-}C_3N_4$-based Z-scheme photocatalysts, researchers have made many attempts to explore other candidates to fabricate $g\text{-}C_3N_4$-based Z-scheme systems, *e.g.*, $g\text{-}C_3N_4/ZnO$,[248] $CdS/RGO/g\text{-}C_3N_4$,[249] $g\text{-}C_3N_4$–RGO–TiO_2,[250] $MoO_3/g\text{-}C_3N_4$,[251] $Cu_3P/g\text{-}C_3N_4$,[252] $NiTiO_3/g\text{-}C_3N_4$,[253] $LaFeO_3/g\text{-}C_3N_4$,[120] $V_2O_5/g\text{-}C_3N_4$,[107] $SnO_{2x}/g\text{-}C_3N_4$,[254] $InVO_4/Bi_2S_3/g\text{-}C_3N_4$,[255] $CDs/g\text{-}C_3N_4/SnO_2$,[256] $g\text{-}C_3N_4/ZnFe_2O_4/UiO\text{-}66$,[256] and $g\text{-}C_3N_4/BiVO_4/CoFe_2O_4$.[257] They have been extensively utilized as an efficient visible-light-guided photocatalyst with enhanced photocatalytic degradation activity. The recovery of the photocatalyst is also very important for efficient removal. Thus, the magnetic $g\text{-}C_3N_4$-based Z-scheme photocatalysts[258,259] are also very useful in this field. The use of $g\text{-}C_3N_4$-based Z-scheme photocatalysts to degrade organic pollutions in actual water bodies is also very important.[260] Of course, a more in-depth comprehension of the charge transfer route and photocatalytic mechanism is crucial for further clarification and amelioration. Some theoretical calculations and advanced characterization techniques, such as *in situ* FTIR, *in situ* XPS, and synchrotron radiation, are vital for further providing the specific charge transfer route and photocatalytic mechanism. Beyond question, $g\text{-}C_3N_4$-based Z-scheme systems will have enormous potential in photocatalytic organic pollutant degradation.

6. Conclusions and outlook

g-C_3N_4-based photocatalysts have attracted increasing interests because of their easy functionalization, suitable band structure, outstanding physicochemical stability and high photocatalytic property. However, the fast charge recombination and low light utilization greatly limit their practical organic pollution removal application. Luckily, g-C_3N_4-based Z-scheme photocatalysts can greatly boost the spatial separation of the photogenerated carrier and enhance their photocatalytic activity and light utilization. Thus, g-C_3N_4-based Z-scheme photocatalysts exhibit great potential for organic pollution removal. Although many achievements have been obtained, the research studies on g-C_3N_4-based Z-scheme photocatalysts are still at their initial stage, and further explorations are evidently needed. Some opportunities and challenges need to be further emphasized and explored, as shown below:

(1) A more in-depth comprehension of the charge transfer route and photocatalytic mechanism is crucial for further clarification and amelioration. Some theoretical calculations and characterization techniques, such as *in situ* FTIR, *in situ* XPS, and synchrotron radiation, are vital for further providing the specific charge transfer route and photocatalytic mechanism. Additionally, the step-scheme (S-scheme) mechanism[261] is more reasonable and powerful for illustrating the evidently improved photocatalytic property.

(2) The physicochemical property of the g-C_3N_4-based Z-scheme photocatalysts should be further optimized. The main attempts should concentrate on the construction of advanced semiconductors with high light utilization efficiency, low charge-carrier-transfer resistance, and good physicochemical stability. In addition, dimension engineering (*e.g.*, 0D quantum dots, 1D nanowires and nanorods, 2D nanosheets and 3D sphere and core–shell, *etc.*) should be considered more.

(3) The crystalline structure of g-C_3N_4-based Z-scheme photocatalysts is also vital for the enhanced charge migration efficiency. Normally, the transfer efficiency of photogenerated charges will be greatly decreased owing to the defects, mismatch of lattice parameters, and electronic configurations. Therefore, the optimization of the crystalline structure of the g-C_3N_4-based Z-scheme photocatalysts is a promising method for improving their photocatalytic performance.

(4) The photocatalytic performance of g-C_3N_4-based Z-scheme systems can be further improved *via* fabricating ternary or multicomponent systems. A practical method is to load suitable co-catalysts on the g-C_3N_4-based Z-scheme photocatalysts that will be very good for further enhancing its e^-–h^+ separation and light utilization.

(5) Considering the unique advantages of g-C_3N_4-based Z-scheme systems, widening their application scope (*i.e.*, energy gas conversion, desulfurization, organic photosynthesis) is critical to building a sustainable society.

(6) In regard to g-C_3N_4-based Z-scheme systems for organic pollution removal, only considering the photocatalytic property is not enough. Other aspects, including cost, environment, and ecology, should also be focused on.

(7) In order to achieving a practical application of g-C_3N_4-based Z-scheme systems, some efficient enhancement approaches, *e.g.*, morphology regulation, loading co-catalysts, interface engineering, doping and vacancy, and exposing more reactive facets, should be highly considered.

Looking to the future, there has been a lot of opportunities and challenges for g-C_3N_4-based Z-scheme photocatalysts for organic pollution removal. It is believed that this review can provide some new and advanced insights for guiding the rational design of g-C_3N_4-based Z-scheme systems for organic pollution removal. Certainly, the g-C_3N_4-based Z-scheme systems can achieve practical industrial applications in the near future.

Conflicts of interest

There are no conflicts of interest to declare.

Acknowledgements

This work was supported by the National Natural Science Foundation of China (Grant No. 52203110), the Knowledge Innovation Program of Wuhan-Shuguang Project (Grant No. 2022010801020216), the Scientific Research Foundation of Fujian University of Technology (Grant No. GY-Z220182), the China Postdoctoral Science Foundation (Grant No. 2021M693795), and the Excellent Youth Foundation of Jiangsu Science Committee (Grant No. BK20220118).

References

1 Q. Wu, J. Wang, Z. Wang, Y. Xu, Z. Xing, X. Zhang, Y. Guan, G. Liao and X. Li, *J. Mater. Chem. A*, 2020, **8**, 13685–13693.
2 H. Zhu, S. Cai, G. Liao, Z. F. Gao, X. Min, Y. Huang, S. Jin and F. Xia, *ACS Catal.*, 2021, **11**, 14751–14771.
3 Y. Zhang, J. Cheng, Y. Xing, Z. Tan, G. Liao and S. Liu, *Mater. Sci. Semicond. Process.*, 2023, **161**, 107463.
4 Z. Li, J. Zhang, Y. Huang, J. Zhai, G. Liao, Z. Wang and C. Ning, *Coord. Chem. Rev.*, 2022, **471**, 214723.
5 R. Jia, C. He, Q. Li, S.-Y. Liu and G. Liao, *Trends Biotechnol.*, 2022, **40**, 1425–1438.
6 S. Liu, Y. Guo, S. Yi, S. Yan, C. Ouyang, F. Deng, C. Li, G. Liao and Q. Li, *Sep. Purif. Technol.*, 2023, **307**, 122727.
7 W. Xiao, X. Jiang, X. Liu, W. Zhou, Z. N. Garba, I. Lawan, L. Wang and Z. Yuan, *J. Cleaner Prod.*, 2021, **284**, 124773.
8 Z. Yan, T. Wu, G. Fang, M. Ran, K. Shen and G. Liao, *RSC Adv.*, 2021, **11**, 4713–4722.
9 G. Liao, L. Zhong, C. S. Cheung, C. Du, J. Wu, W. Du, H. Zheng and H. Gao, *Microporous Mesoporous Mater.*, 2020, **307**, 110469.

10 D. Pathania, S. Sharma and P. Singh, *Arabian J. Chem.*, 2017, **10**, S1445–S1451.
11 Z. Wang, A. Berbille, Y. Feng, S. Li, L. Zhu, W. Tang and Z. L. Wang, *Nat. Commun.*, 2022, **13**, 130.
12 X. Ma, L. Xing, K. Liu and L. Liu, *Catal. Sci. Technol.*, 2023, **13**, 788–801.
13 C. Li, H. Che, C. Liu, G. Che, P. A. Charpentier, W. Z. Xu, X. Wang and L. Liu, *J. Taiwan Inst. Chem. Eng.*, 2019, **95**, 669–681.
14 R. Acharya, B. Naik and K. Parida, *Beilstein J. Nanotechnol.*, 2018, **9**, 1448–1470.
15 F. Tian, X. Wu, S. Liu, Y. Gu, Z. Lin, H. Zhang, X. Yan and G. Liao, *Sustainable Energy Fuels*, 2023, **7**, 786–796.
16 J.-Z. Cheng, L.-L. Liu, G. Liao, Z.-Q. Shen, Z.-R. Tan, Y.-Q. Xing, X.-X. Li, K. Yang, L. Chen and S.-Y. Liu, *J. Mater. Chem. A*, 2020, **8**, 5890–5899.
17 C. Li, H. Che, P. Huo, Y. Yan, C. Liu and H. Dong, *J. Colloid Interface Sci.*, 2021, **581**, 764–773.
18 C. Li, X. Liu, Y. Yan, X. Song, Y. Yan, C. Liu, R. Xu and P. Huo, *Chem. Eng. J.*, 2021, **410**, 128316.
19 C. Li, Y. Zhao, X. Liu, P. Huo, Y. Yan, L. Wang, G. Liao and C. Liu, *J. Colloid Interface Sci.*, 2021, **600**, 794–803.
20 R. Acharya and P. Pani, *Mater. Today: Proc.*, 2022, **67**, 1276–1282.
21 R. Acharya, L. Acharya and K. Parida, in *Perovskite Materials for Energy and Environmental Applications*, 2022, pp. 167–216.
22 V. Hasija, A. Kumar, A. Sudhaik, P. Raizada, P. Singh, Q. Van Le, T. T. Le and V.-H. Nguyen, *Environ. Chem. Lett.*, 2021, **19**, 2941–2966.
23 A. Kumar, P. Raizada, A. Hosseini-Bandegharaei, V. K. Thakur, V.-H. Nguyen and P. Singh, *J. Mater. Chem. A*, 2021, **9**, 111–153.
24 C. Li, H. Che, Y. Yan, C. Liu and H. Dong, *Chem. Eng. J.*, 2020, **398**, 125523.
25 S. Li, S. Shan, S. Chen, H. Li, Z. Li, Y. Liang, J. Fei, L. Xie and J. Li, *J. Environ. Chem. Eng.*, 2021, **9**, 105967.
26 C. Li, X. Liu, P. Huo, Y. Yan, G. Liao, G. Ding and C. Liu, *Small*, 2021, **17**, 2102539.
27 C. Li, G. Ding, X. Liu, P. Huo, Y. Yan, Y. Yan and G. Liao, *Chem. Eng. J.*, 2022, **435**, 134740.
28 C. Li, X. Liu, G. Ding, P. Huo, Y. Yan, Y. Yan and G. Liao, *Inorg. Chem.*, 2022, **61**, 4681–4689.
29 B. Yang, X. Li, Q. Zhang, X. Yang, J. Wan, G. Liao, J. Zhao, R. Wang, J. Liu, R. D. Rodriguez and X. Jia, *Appl. Catal., B*, 2022, **314**, 121521.
30 B. Yang, Z. Wang, J. Zhao, X. Sun, R. Wang, G. Liao and X. Jia, *Int. J. Hydrogen Energy*, 2021, **46**, 25436–25447.
31 Z.-R. Tan, Y.-Q. Xing, J.-Z. Cheng, G. Zhang, Z.-Q. Shen, Y.-J. Zhang, G. Liao, L. Chen and S.-Y. Liu, *Chem. Sci.*, 2022, **13**, 1725–1733.
32 G. Liao, Y. Gong, L. Zhang, H. Gao, G.-J. Yang and B. Fang, *Energy Environ. Sci.*, 2019, **12**, 2080–2147.
33 W.-J. Ong, L.-L. Tan, Y. H. Ng, S.-T. Yong and S.-P. Chai, *Chem. Rev.*, 2016, **116**, 7159–7329.
34 G. Liao, F. He, Q. Li, L. Zhong, R. Zhao, H. Che, H. Gao and B. Fang, *Prog. Mater. Sci.*, 2020, **112**, 100666.
35 G. Liao, C. Li, X. Li and B. Fang, *Cell Rep. Phys. Sci.*, 2021, **2**, 100355.
36 B. Yang, J. Han, Q. Zhang, G. Liao, W. Cheng, G. Ge, J. Liu, X. Yang, R. Wang and X. Jia, *Carbon*, 2023, **202**, 348–357.
37 F. Su, Z. Wang, H. Cao, H. Xie, W. Tu, Y. Xiao, S. Shi, J. Chen, X. Jin and X. Y. Kong, *Catal. Sci. Technol.*, 2023, **13**, 1325–1334.
38 V. Hasija, P. Raizada, A. Sudhaik, K. Sharma, A. Kumar, P. Singh, S. B. Jonnalagadda and V. K. Thakur, *Appl. Mater. Today*, 2019, **15**, 494–524.
39 T. Wu, Q. He, Z. Liu, B. Shao, Q. Liang, Y. Pan, J. Huang, Z. Peng, Y. Liu, C. Zhao, X. Yuan, L. Tang and S. Gong, *J. Hazard. Mater.*, 2022, **424**, 127177.
40 Y. Pan, X. Liu, W. Zhang, B. Shao, Z. Liu, Q. Liang, T. Wu, Q. He, J. Huang, Z. Peng, Y. Liu and C. Zhao, *Chem. Eng. J.*, 2022, **427**, 132032.
41 Q. Liang, X. Liu, B. Shao, L. Tang, Z. Liu, W. Zhang, S. Gong, Y. Liu, Q. He, T. Wu, Y. Pan and S. Tong, *Chem. Eng. J.*, 2021, **426**, 130831.
42 Q. Liang, B. Shao, S. Tong, Z. Liu, L. Tang, Y. Liu, M. Cheng, Q. He, T. Wu, Y. Pan, J. Huang and Z. Peng, *Chem. Eng. J.*, 2021, **405**, 126951.
43 Z. Zhou, Y. Zhang, Y. Shen, S. Liu and Y. Zhang, *Chem. Soc. Rev.*, 2018, **47**, 2298–2321.
44 Y. Bai, Y. Zheng, Z. Wang, Q. Hong, S. Liu, Y. Shen and Y. Zhang, *New J. Chem.*, 2021, **45**, 11876–11892.
45 H. Yang, Z. Wang, S. Liu, Y. Shen and Y. Zhang, *Chin. Chem. Lett.*, 2020, **31**, 3047–3054.
46 H. L. Tan, F. F. Abdi and Y. H. Ng, *Chem. Soc. Rev.*, 2019, **48**, 1255–1271.
47 S. Wang, G. Liu and L. Wang, *Chem. Rev.*, 2019, **119**, 5192–5247.
48 B. He, M. Feng, X. Chen, D. Zhao and J. Sun, *Appl. Surf. Sci.*, 2020, **527**, 146737.
49 G. Liao, C. Li, S.-Y. Liu, B. Fang and H. Yang, *Phys. Rep.*, 2022, **983**, 1–41.
50 G. Liao, C. Li, S.-Y. Liu, B. Fang and H. Yang, *Trends Chem.*, 2022, **4**, 111–127.
51 C. Bie, B. Cheng, J. Fan, W. Ho and J. Yu, *EnergyChem*, 2021, **3**, 100051.
52 J. Fu, B. Zhu, C. Jiang, B. Cheng, W. You and J. Yu, *Small*, 2017, **13**, 1603938.
53 Y. Jiang, Z. Sun, C. Tang, Y. Zhou, L. Zeng and L. Huang, *Appl. Catal., B*, 2019, **240**, 30–38.
54 H. Che, C. Liu, G. Che, G. Liao, H. Dong, C. Li, N. Song and C. Li, *Nano Energy*, 2020, **67**, 104273.
55 X. Chen, R. Shi, Q. Chen, Z. Zhang, W. Jiang, Y. Zhu and T. Zhang, *Nano Energy*, 2019, **59**, 644–650.
56 K. Schwinghammer, M. B. Mesch, V. Duppel, C. Ziegler, J. Senker and B. V. Lotsch, *J. Am. Chem. Soc.*, 2014, **136**, 1730–1733.
57 O. Fontelles-Carceller, M. J. Muñoz-Batista, M. Fernández-García and A. Kubacka, *ACS Appl. Mater. Interfaces*, 2016, **8**, 2617–2627.

58 J. Xue, S. Ma, Y. Zhou, Z. Zhang and M. He, *ACS Appl. Mater. Interfaces*, 2015, **7**, 9630–9637.
59 X.-J. Wang, W.-Y. Yang, F.-T. Li, Y.-B. Xue, R.-H. Liu and Y.-J. Hao, *Ind. Eng. Chem. Res.*, 2013, **52**, 17140–17150.
60 K. Wang, J. Li and G. Zhang, *ACS Appl. Mater. Interfaces*, 2019, **11**, 27686–27696.
61 J. Wang, Y. Chen, Y. Shen, S. Liu and Y. Zhang, *Chem. Commun.*, 2017, **53**, 2978–2981.
62 L. Acharya, S. P. Pattnaik, A. Behera, R. Acharya and K. Parida, *Inorg. Chem.*, 2021, **60**, 5021–5033.
63 S. P. Pattnaik, A. Behera, S. Martha, R. Acharya and K. Parida, *J. Mater. Sci.*, 2019, **54**, 5726–5742.
64 L. Acharya, B. P. Mishra, S. P. Pattnaik, R. Acharya and K. Parida, *New J. Chem.*, 2022, **46**, 3493–3503.
65 Z. Wang, M. Xiao, J. You, G. Liu and L. Wang, *Acc. Mater. Res.*, 2022, **3**, 1127–1136.
66 J. Ma, X. Peng, Z. Zhou, H. Yang, K. Wu, Z. Fang, D. Han, Y. Fang, S. Liu, Y. Shen and Y. Zhang, *Angew. Chem., Int. Ed.*, 2022, **61**, e202210856.
67 P. Kumar, E. Vahidzadeh, U. K. Thakur, P. Kar, K. M. Alam, A. Goswami, N. Mahdi, K. Cui, G. M. Bernard, V. K. Michaelis and K. Shankar, *J. Am. Chem. Soc.*, 2019, **141**, 5415–5436.
68 H. Yang, Q. Zhou, Z. Fang, W. Li, Y. Zheng, J. Ma, Z. Wang, L. Zhao, S. Liu, Y. Shen and Y. Zhang, *Chem*, 2021, **7**, 2708–2721.
69 J. Mahmood, E. K. Lee, M. Jung, D. Shin, H.-J. Choi, J.-M. Seo, S.-M. Jung, D. Kim, F. Li, M. S. Lah, N. Park, H.-J. Shin, J. H. Oh and J.-B. Baek, *Proc. Natl. Acad. Sci. U. S. A.*, 2016, **113**, 7414–7419.
70 H. Wang, L. Zhang, Z. Chen, J. Hu, S. Li, Z. Wang, J. Liu and X. Wang, *Chem. Soc. Rev.*, 2014, **43**, 5234–5244.
71 J. Fu, J. Yu, C. Jiang and B. Cheng, *Adv. Energy Mater.*, 2018, **8**, 1701503.
72 J. Low, J. Yu, M. Jaroniec, S. Wageh and A. A. Al-Ghamdi, *Adv. Mater.*, 2017, **29**, 1601694.
73 J. Yu, S. Wang, J. Low and W. Xiao, *Phys. Chem. Chem. Phys.*, 2013, **15**, 16883–16890.
74 J. Low, C. Jiang, B. Cheng, S. Wageh, A. A. Al-Ghamdi and J. Yu, *Small Methods*, 2017, **1**, 1700080.
75 K. Qi, B. Cheng, J. Yu and W. Ho, *Chin. J. Catal.*, 2017, **38**, 1936–1955.
76 Q. Xu, L. Zhang, J. Yu, S. Wageh, A. A. Al-Ghamdi and M. Jaroniec, *Mater. Today*, 2018, **21**, 1042–1063.
77 J. Wen, J. Xie, X. Chen and X. Li, *Appl. Surf. Sci.*, 2017, **391**, 72–123.
78 D. Masih, Y. Ma and S. Rohani, *Appl. Catal., B*, 2017, **206**, 556–588.
79 Z. Zhao, Y. Sun and F. Dong, *Nanoscale*, 2015, **7**, 15–37.
80 M. Inagaki, T. Tsumura, T. Kinumoto and M. Toyoda, *Carbon*, 2019, **141**, 580–607.
81 B. Zhu, L. Zhang, B. Cheng and J. Yu, *Appl. Catal., B*, 2018, **224**, 983–999.
82 S. Zhang, P. Gu, R. Ma, C. Luo, T. Wen, G. Zhao, W. Cheng and X. Wang, *Catal. Today*, 2019, **335**, 65–77.
83 M. Xiao, B. Luo, S. Wang and L. Wang, *J. Energy Chem.*, 2018, **27**, 1111–1123.
84 C. Zhang, Y. Li, D. Shuai, Y. Shen, W. Xiong and L. Wang, *Chemosphere*, 2019, **214**, 462–479.
85 A. Nikokavoura and C. Trapalis, *Appl. Surf. Sci.*, 2018, **430**, 18–52.
86 F. Bairamis, I. Rapti and I. Konstantinou, *Curr. Opin. Green Sustainable Chem.*, 2022, 100749.
87 J. Jia, Q. Zhang, K. Li, Y. Zhang, E. Liu and X. Li, *Int. J. Hydrogen Energy*, 2023, **48**, 196–231.
88 J. Fernández-Catalá, R. Greco, M. Navlani-García, W. Cao, Á. Berenguer-Murcia and D. Cazorla-Amorós, *Catalysts*, 2022, **12**, 1137.
89 M. Li, L. Zhang, M. Wu, Y. Du, X. Fan, M. Wang, L. Zhang, Q. Kong and J. Shi, *Nano Energy*, 2016, **19**, 145–155.
90 P. Qiu, H. Chen and F. Jiang, *RSC Adv.*, 2014, **4**, 39969–39977.
91 J. Chen, S. Shen, P. Guo, M. Wang, P. Wu, X. Wang and L. Guo, *Appl. Catal., B*, 2014, **152–153**, 335–341.
92 X. Liu, A. Jin, Y. Jia, J. Jiang, N. Hu and X. Chen, *RSC Adv.*, 2015, **5**, 92033–92041.
93 J. Zhang, M. Zhang, R.-Q. Sun and X. Wang, *Angew. Chem., Int. Ed.*, 2012, **51**, 10145–10149.
94 L. Sun, W. Wang, C. Zhang, M. Cheng, Y. Zhou, Y. Yang, H. Luo, D. Qin, C. Huang and Z. Ouyang, *Chem. Eng. J.*, 2022, **446**, 137027.
95 T. Su, Z. Qin, H. Ji and Z. Wu, *Nanotechnology*, 2019, **30**, 502002.
96 K. Li, F.-Y. Su and W.-D. Zhang, *Appl. Surf. Sci.*, 2016, **375**, 110–117.
97 X. Li, J. Yu, J. Low, Y. Fang, J. Xiao and X. Chen, *J. Mater. Chem. A*, 2015, **3**, 2485–2534.
98 T. Su, Q. Shao, Z. Qin, Z. Guo and Z. Wu, *ACS Catal.*, 2018, **8**, 2253–2276.
99 S. J. A. Moniz, S. A. Shevlin, D. J. Martin, Z.-X. Guo and J. Tang, *Energy Environ. Sci.*, 2015, **8**, 731–759.
100 K. Maeda, *ACS Catal.*, 2013, **3**, 1486–1503.
101 Z. Li, G. Weng, Q. Zou, G. Cong and Y.-C. Lu, *Nano Energy*, 2016, **30**, 283–292.
102 D. Huang, S. Chen, G. Zeng, X. Gong, C. Zhou, M. Cheng, W. Xue, X. Yan and J. Li, *Coord. Chem. Rev.*, 2019, **385**, 44–80.
103 X. Cao, Z. Chen, R. Lin, W.-C. Cheong, S. Liu, J. Zhang, Q. Peng, C. Chen, T. Han, X. Tong, Y. Wang, R. Shen, W. Zhu, D. Wang and Y. Li, *Nat. Catal.*, 2018, **1**, 704–710.
104 Y.-C. Zhang, N. Afzal, L. Pan, X. Zhang and J.-J. Zou, *Adv. Sci.*, 2019, **6**, 1900053.
105 R. He, D. Xu, B. Cheng, J. Yu and W. Ho, *Nanoscale Horiz.*, 2018, **3**, 464–504.
106 D. Zheng, C. Pang and X. Wang, *Chem. Commun.*, 2015, **51**, 17467–17470.
107 Y. Hong, Y. Jiang, C. Li, W. Fan, X. Yan, M. Yan and W. Shi, *Appl. Catal., B*, 2016, **180**, 663–673.
108 W. Yu, D. Xu and T. Peng, *J. Mater. Chem. A*, 2015, **3**, 19936–19947.

109 K. Kailasam, A. Fischer, G. Zhang, J. Zhang, M. Schwarze, M. Schröder, X. Wang, R. Schomäcker and A. Thomas, *ChemSusChem*, 2015, **8**, 1404–1410.
110 S. Meng, X. Ning, T. Zhang, S.-F. Chen and X. Fu, *Phys. Chem. Chem. Phys.*, 2015, **17**, 11577–11585.
111 N. Tian, H. Huang, Y. He, Y. Guo, T. Zhang and Y. Zhang, *Dalton Trans.*, 2015, **44**, 4297–4307.
112 M. Li, L. Zhang, X. Fan, Y. Zhou, M. Wu and J. Shi, *J. Mater. Chem. A*, 2015, **3**, 5189–5196.
113 Y. Bai, P.-Q. Wang, J.-Y. Liu and X.-J. Liu, *RSC Adv.*, 2014, **4**, 19456–19461.
114 Y. Feng, J. Shen, Q. Cai, H. Yang and Q. Shen, *New J. Chem.*, 2015, **39**, 1132–1138.
115 H. Cheng, J. Hou, O. Takeda, X.-M. Guo and H. Zhu, *J. Mater. Chem. A*, 2015, **3**, 11006–11013.
116 H. Li, H. Yu, X. Quan, S. Chen and Y. Zhang, *ACS Appl. Mater. Interfaces*, 2016, **8**, 2111–2119.
117 Y. Yang, W. Guo, Y. Guo, Y. Zhao, X. Yuan and Y. Guo, *J. Hazard. Mater.*, 2014, **271**, 150–159.
118 F. Shi, L. Chen, M. Chen and D. Jiang, *Chem. Commun.*, 2015, **51**, 17144–17147.
119 W. Yin, L. Bai, Y. Zhu, S. Zhong, L. Zhao, Z. Li and S. Bai, *ACS Appl. Mater. Interfaces*, 2016, **8**, 23133–23142.
120 Y. Wu, H. Wang, W. Tu, Y. Liu, Y. Z. Tan, X. Yuan and J. W. Chew, *J. Hazard. Mater.*, 2018, **347**, 412–422.
121 S. Shenoy, C. Chuaicham, T. Okumura, K. Sekar and K. Sasaki, *Chem. Eng. J.*, 2023, **453**, 139758.
122 C. Liu, S. Sun, M. Yu, Y. Zhou, X. Zhang and J. Niu, *Sep. Purif. Technol.*, 2023, **311**, 123359.
123 L. Sruthi, B. Janani and S. Sudheer Khan, *Sep. Purif. Technol.*, 2021, **279**, 119709.
124 S. Zhu and D. Wang, *Adv. Energy Mater.*, 2017, **7**, 1700841.
125 T. Di, Q. Xu, W. Ho, H. Tang, Q. Xiang and J. Yu, *ChemCatChem*, 2019, **11**, 1394–1411.
126 J. K. Stolarczyk, S. Bhattacharyya, L. Polavarapu and J. Feldmann, *ACS Catal.*, 2018, **8**, 3602–3635.
127 W. Yu, J. Chen, T. Shang, L. Chen, L. Gu and T. Peng, *Appl. Catal., B*, 2017, **219**, 693–704.
128 R. Ye, H. Fang, Y.-Z. Zheng, N. Li, Y. Wang and X. Tao, *ACS Appl. Mater. Interfaces*, 2016, **8**, 13879–13889.
129 K. Wenderich and G. Mul, *Chem. Rev.*, 2016, **116**, 14587–14619.
130 Q. Xu, B. Zhu, C. Jiang, B. Cheng and J. Yu, *Sol. RRL*, 2018, **2**, 1800006.
131 G. Liao, L. Zhang, C. Li, S.-Y. Liu, B. Fang and H. Yang, *Matter*, 2022, **5**, 3341–3374.
132 X. Li, T. Liu, Y. Zhang, J. Cai, M. He, M. Li, Z. Chen and L. Zhang, *Adv. Fiber Mater.*, 2022, **4**, 1620–1631.
133 H. Zhai, Z. Liu, L. Xu, T. Liu, Y. Fan, L. Jin, R. Dong, Y. Yi and Y. Li, *Adv. Fiber Mater.*, 2022, **4**, 1595–1608.
134 Z. Qin, M. Qiu, Q. Zhang, S. Yang, G. Liao, Z. Xiong and Z. Xu, *J. Mater. Chem. B*, 2021, **9**, 8882–8896.
135 Y. Zou, F. Sun, C. Liu, C. Yu, M. Zhang, Q. He, Y. Xiong, Z. Xu, S. Yang and G. Liao, *Chem. Eng. J.*, 2019, **357**, 237–247.
136 Y. Zhao, G. I. N. Waterhouse, G. Chen, X. Xiong, L.-Z. Wu, C.-H. Tung and T. Zhang, *Chem. Soc. Rev.*, 2019, **48**, 1972–2010.
137 P. Xia, B. Zhu, B. Cheng, J. Yu and J. Xu, *ACS Sustainable Chem. Eng.*, 2018, **6**, 965–973.
138 R. Acharya, S. Pati and K. Parida, *J. Mol. Liq.*, 2022, **357**, 119105.
139 H. S. Moon, K.-C. Hsiao, M.-C. Wu, Y. Yun, Y.-J. Hsu and K. Yong, *Adv. Mater.*, 2023, **35**, 2200172.
140 H. Li, Y. Gao, Y. Zhou, F. Fan, Q. Han, Q. Xu, X. Wang, M. Xiao, C. Li and Z. Zou, *Nano Lett.*, 2016, **16**, 5547–5552.
141 Y. Jiang, H.-Y. Chen, J.-Y. Li, J.-F. Liao, H.-H. Zhang, X.-D. Wang and D.-B. Kuang, *Adv. Funct. Mater.*, 2020, **30**, 2004293.
142 X. Xia, M. Song, H. Wang, X. Zhang, N. Sui, Q. Zhang, V. L. Colvin and W. Y. William, *Nanoscale*, 2019, **11**, 11071–11082.
143 Y. Jiang, J.-F. Liao, H.-Y. Chen, H.-H. Zhang, J.-Y. Li, X.-D. Wang and D.-B. Kuang, *Chem*, 2020, **6**, 766–780.
144 R. Chen, H. Yin, L. Wang, Z. Zhang, J. Ding, J. Zhang, H. Wan and G. Guan, *J. Colloid Interface Sci.*, 2023, **631**, 122–132.
145 B. Nian, G. Liao, Y. Song, Y. Su, C. Cao and Y. Liu, *J. Catal.*, 2020, **384**, 159–168.
146 G. Liao, Z. Xiao, X. Chen, C. Du, L. Zhong, C. S. Cheung and H. Gao, *Macromolecules*, 2020, **53**, 256–266.
147 W. Yu, J. Zhang and T. Peng, *Appl. Catal., B*, 2016, **181**, 220–227.
148 X. Wang, J. Song, Y. Lu, W. Zhu and G. Hu, *J. Mater. Sci.: Mater. Electron.*, 2021, **32**, 2061–2074.
149 P. Murugesan, S. Narayanan, M. Manickam, P. K. Murugesan and R. Subbiah, *Appl. Surf. Sci.*, 2018, **450**, 516–526.
150 F. Wang, W. Li, S. Gu, H. Li, X. Wu, C. Ren and X. Liu, *J. Photochem. Photobiol., A*, 2017, **335**, 140–148.
151 A. H. Mamaghani, F. Haghighat and C.-S. Lee, *Appl. Catal., B*, 2020, **269**, 118735.
152 Q. Li, G. Liao, S. Zhang, L. Pang, H. Tong, W. Zhao and Z. Xu, *Appl. Surf. Sci.*, 2018, **427**, 437–450.
153 P. Xu and G. Liao, *Materials*, 2018, **11**, 1616.
154 Z. Mo, X. Pan, X. Pan, L. Ye, H. Hu, Q. Xu, X. Hu, Z. Xu, J. Xiong, G. Liao and S. Yang, *J. Mater. Chem. B*, 2022, **10**, 8760–8770.
155 L. Zhang, G. Oudeng, F. Wen and G. Liao, *Biomater. Res.*, 2022, **26**, 61.
156 W. Chen, T.-Y. Liu, T. Huang, X.-H. Liu, J.-W. Zhu, G.-R. Duan and X.-J. Yang, *Appl. Surf. Sci.*, 2015, **355**, 379–387.
157 S. T. Aruna and A. S. Mukasyan, *Curr. Opin. Solid State Mater. Sci.*, 2008, **12**, 44–50.
158 X. Xia, M. Song, H. Wang, X. Zhang, N. Sui, Q. Zhang, V. L. Colvin and W. W. Yu, *Nanoscale*, 2019, **11**, 11071–11082.
159 L. Jiang, X. Yuan, G. Zeng, J. Liang, X. Chen, H. Yu, H. Wang, Z. Wu, J. Zhang and T. Xiong, *Appl. Catal., B*, 2018, **227**, 376–385.
160 S. Liu, J. Chen, D. Xu, X. Zhang and M. Shen, *J. Mater. Res.*, 2018, **33**, 1391–1400.
161 L. Lu, G. Wang, M. Zou, J. Wang and J. Li, *Appl. Surf. Sci.*, 2018, **441**, 1012–1023.
162 J. B. Rivest and P. K. Jain, *Chem. Soc. Rev.*, 2013, **42**, 89–96.

163 R. K. Khamizov, V. A. Ivanov and A. A. Madani, *React. Funct. Polym.*, 2010, **70**, 521–530.
164 J. Wu, S. Nie, H. Liu, C. Gong, Q. Zhang, Z. Xu and G. Liao, *J. Mater. Chem. A*, 2022, **10**, 19914–19924.
165 H. Zhao, X. Ding, B. Zhang, Y. Li and C. Wang, *Sci. Bull.*, 2017, **62**, 602–609.
166 J. Liang, H. Zhao, L. Yue, G. Fan, T. Li, S. Lu, G. Chen, S. Gao, A. M. Asiri and X. Sun, *J. Mater. Chem. A*, 2020, **8**, 16747–16789.
167 C. Bavatharani, E. Muthusankar, S. M. Wabaidur, Z. A. Alothman, K. M. Alsheetan, M. M. Al-Anazy and D. Ragupathy, *Synth. Met.*, 2021, **271**, 116609.
168 R. C. Pawar, S. Kang, J. H. Park, J.-H. Kim, S. Ahn and C. S. Lee, *Sci. Rep.*, 2016, **6**, 31147.
169 M. Nehra, N. Dilbaghi, G. Marrazza, A. Kaushik, R. Abolhassani, Y. K. Mishra, K. H. Kim and S. Kumar, *Nano Energy*, 2020, **76**, 104991.
170 L. Hu, J. Yan, C. Wang, B. Chai and J. Li, *Chin. J. Catal.*, 2019, **40**, 458–469.
171 H. Cölfen and S. Mann, *Angew. Chem., Int. Ed.*, 2003, **42**, 2350–2365.
172 J. Peet, A. J. Heeger and G. C. Bazan, *Acc. Chem. Res.*, 2009, **42**, 1700–1708.
173 Z. Yan, G. Liao, X. Zou, M. Zhao, T. Wu, Y. Chen and G. Fang, *J. Agric. Food Chem.*, 2020, **68**, 8341–8349.
174 Z. Yan, B. Song, G. Fang, T. Wu, N. Chen, M. Zhao, X. Zou and G. Liao, *ACS Sustainable Chem. Eng.*, 2021, **9**, 10403–10423.
175 N. Nie, L. Zhang, J. Fu, B. Cheng and J. Yu, *Appl. Surf. Sci.*, 2018, **441**, 12–22.
176 S. Kumar, A. Baruah, S. Tonda, B. Kumar, V. Shanker and B. Sreedhar, *Nanoscale*, 2014, **6**, 4830–4842.
177 Y. Lin, S. Yang, Y. Liu, S. Zhang, H. Wang, H. Yu and F. Peng, *Int. J. Hydrogen Energy*, 2017, **42**, 19942–19950.
178 Z. Gan, C. Huang, Y. Shen, Q. Zhou, D. Han, J. Ma, S. Liu and Y. Zhang, *Chin. Chem. Lett.*, 2020, **31**, 513–516.
179 C. Huang, Y. Wen, J. Ma, D. Dong, Y. Shen, S. Liu, H. Ma and Y. Zhang, *Nat. Commun.*, 2021, **12**, 320.
180 R. He, J. Zhou, H. Fu, S. Zhang and C. Jiang, *Appl. Surf. Sci.*, 2018, **430**, 273–282.
181 Y. Xue, Z. Wu, X. He, Q. Li, X. Yang and L. Li, *J. Colloid Interface Sci.*, 2019, **548**, 293–302.
182 D. Ni, H. Shen, H. Li, Y. Ma and T. Zhai, *Appl. Surf. Sci.*, 2017, **409**, 241–249.
183 D. Zhou, B. Yu, Q. Chen, H. Shi, Y. Zhang, D. Li, X. Yang, W. Zhao, C. Liu, G. Wei and Z. Chen, *Mater. Res. Bull.*, 2020, **124**, 110757.
184 A. Abdolhoseinzadeh and S. Sheibani, *Adv. Powder Technol.*, 2020, **31**, 40–50.
185 D. Majhi, K. Das, R. Bariki, S. Padhan, A. Mishra, R. Dhiman, P. Dash, B. Nayak and B. G. Mishra, *J. Mater. Chem. A*, 2020, **8**, 21729–21743.
186 M. S. Khan, F. Zhang, M. Osada, S. S. Mao and S. Shen, *Sol. RRL*, 2020, **4**, 1900435.
187 T. Ohno, N. Murakami, T. Koyanagi and Y. Yang, *J. CO2 Util.*, 2014, **6**, 17–25.
188 U. Ghosh and A. Pal, *J. Ind. Eng. Chem.*, 2019, **79**, 383–408.
189 M. Pang, J. Hu and H. C. Zeng, *J. Am. Chem. Soc.*, 2010, **132**, 10771–10785.
190 T. Zhang, M. Long, K. Yan, M. Qin, X. Lu, X. Zeng, C. M. Cheng, K. S. Wong, P. Liu, W. Xie and J. Xu, *Adv. Energy Mater.*, 2017, **7**, 1700118.
191 W. Deng, X. Zhang, H. Dong, J. Jie, X. Xu, J. Liu, L. He, L. Xu, W. Hu and X. Zhang, *Mater. Today*, 2019, **24**, 17–25.
192 D. F. Fletcher and G. J. Brown, *Int. J. Comput. Fluid Dyn.*, 2009, **23**, 173–187.
193 R. Das, C. D. Vecitis, A. Schulze, B. Cao, A. F. Ismail, X. Lu, J. Chen and S. Ramakrishna, *Chem. Soc. Rev.*, 2017, **46**, 6946–7020.
194 G. Liao, J. Chen, W. Zeng, C. Yu, C. Yi and Z. Xu, *J. Phys. Chem. C*, 2016, **120**, 25935–25944.
195 G. Liao, Q. Li, W. Zhao, Q. Pang, H. Gao and Z. Xu, *Appl. Catal., A*, 2018, **549**, 102–111.
196 G. Liao, J. Fang, Q. Li, S. Li, Z. Xu and B. Fang, *Nanoscale*, 2019, **11**, 7062–7096.
197 G. Liao, W. Zhao, Q. Li, Q. Pang and Z. Xu, *Chem. Lett.*, 2017, **46**, 1631–1634.
198 G. Liao, Y. Gong, L. Zhong, J. Fang, L. Zhang, Z. Xu, H. Gao and B. Fang, *Nano Res.*, 2019, **12**, 2407–2436.
199 H. Zhu, C. Zhang, K. Xie, X. Li and G. Liao, *Chem. Eng. J.*, 2023, **453**, 139775.
200 L. Acharya, S. Nayak, S. P. Pattnaik, R. Acharya and K. Parida, *J. Colloid Interface Sci.*, 2020, **566**, 211–223.
201 X. Zhang, S. Tong, D. Huang, Z. Liu, B. Shao, Q. Liang, T. Wu, Y. Pan, J. Huang, Y. Liu, M. Cheng and M. Chen, *Coord. Chem. Rev.*, 2021, **448**, 214177.
202 M. Z. Rahman and C. B. Mullins, *Acc. Chem. Res.*, 2019, **52**, 248–257.
203 R. Qian, H. Zong, J. Schneider, G. Zhou, T. Zhao, Y. Li, J. Yang, D. W. Bahnemann and J. H. Pan, *Catal. Today*, 2019, **335**, 78–90.
204 G. Liao, X. Tao and B. Fang, *Matter*, 2022, **5**, 377–379.
205 D. Zhou, Z. Chen, Q. Yang, C. Shen, G. Tang, S. Zhao, J. Zhang, D. Chen, Q. Wei and X. Dong, *ChemCatChem*, 2016, **8**, 3064–3073.
206 Y. Li, K. Lv, W. Ho, F. Dong, X. Wu and Y. Xia, *Appl. Catal., B*, 2017, **202**, 611–619.
207 H. L. Tan, X. Wen, R. Amal and Y. H. Ng, *J. Phys. Chem. Lett.*, 2016, **7**, 1400–1405.
208 R. Rajendran, S. Vignesh, S. Suganthi, V. Raj, G. Kavitha, B. Palanivel, M. Shkir and H. Algarni, *J. Phys. Chem. Solids*, 2022, **161**, 110391.
209 Z. A. Huang, Q. Sun, K. Lv, Z. Zhang, M. Li and B. Li, *Appl. Catal., B*, 2015, **164**, 420–427.
210 C. P. Sajan, S. Wageh, A. A. Al-Ghamdi, J. Yu and S. Cao, *Nano Res.*, 2016, **9**, 3–27.
211 A. Srinivasan and M. Miyauchi, *J. Phys. Chem. C*, 2012, **116**, 15421–15426.
212 Z.-F. Huang, J. Song, L. Pan, X. Zhang, L. Wang and J.-J. Zou, *Adv. Mater.*, 2015, **27**, 5309–5327.
213 S. Chen, Y. Hu, X. Jiang, S. Meng and X. Fu, *Mater. Chem. Phys.*, 2015, **149–150**, 512–521.

214 X. Liu, A. Jin, Y. Jia, T. Xia, C. Deng, M. Zhu, C. Chen and X. Chen, *Appl. Surf. Sci.*, 2017, **405**, 359–371.
215 L. Cui, X. Ding, Y. Wang, H. Shi, L. Huang, Y. Zuo and S. Kang, *Appl. Surf. Sci.*, 2017, **391**, 202–210.
216 B. Chai, C. Liu, J. Yan, Z. Ren and Z.-J. Wang, *Appl. Surf. Sci.*, 2018, **448**, 1–8.
217 C. Zhao, F. Ran, L. Dai, C. Li, C. Zheng and C. Si, *Carbohydr. Polym.*, 2021, **255**, 117343.
218 S.-L. Chiam, S.-Y. Pung and F.-Y. Yeoh, *Environ. Sci. Pollut. Res.*, 2020, **27**, 5759–5778.
219 J. Liu, B. Cheng and J. Yu, *Phys. Chem. Chem. Phys.*, 2016, **18**, 31175–31183.
220 L. Sun, Y. Qi, C.-J. Jia, Z. Jin and W. Fan, *Nanoscale*, 2014, **6**, 2649–2659.
221 D. Xu, B. Cheng, S. Cao and J. Yu, *Appl. Catal., B*, 2015, **164**, 380–388.
222 S. Sakthivel and H. Kisch, *Angew. Chem., Int. Ed.*, 2003, **42**, 4908–4911.
223 J. Zhang, Y. Hu, X. Jiang, S. Chen, S. Meng and X. Fu, *J. Hazard. Mater.*, 2014, **280**, 713–722.
224 Y. Yang, B. Tan and C. D. Wood, *J. Mater. Chem. A*, 2016, **4**, 15072–15080.
225 J. Li, H. Yuan and Z. Zhu, *Appl. Surf. Sci.*, 2016, **385**, 34–41.
226 L. Zhang, G. Wang, Z. Xiong, H. Tang and C. Jiang, *Appl. Surf. Sci.*, 2018, **436**, 162–171.
227 M. Sun, Y. Wang, Y. Shao, Y. He, Q. Zeng, H. Liang, T. Yan and B. Du, *J. Colloid Interface Sci.*, 2017, **501**, 123–132.
228 G. Long, J. Ding, L. Xie, R. Sun, M. Chen, Y. Zhou, X. Huang, G. Han, Y. Li and W. Zhao, *Appl. Surf. Sci.*, 2018, **455**, 1010–1018.
229 D. Ma, J. Wu, M. Gao, Y. Xin, T. Ma and Y. Sun, *Chem. Eng. J.*, 2016, **290**, 136–146.
230 B. Chong, L. Chen, W. Wang, D. Han, L. Wang, L. Feng, Q. Li and C. Li, *Mater. Lett.*, 2017, **204**, 149–153.
231 H. Che, G. Che, H. Dong, W. Hu, H. Hu, C. Liu and C. Li, *Appl. Surf. Sci.*, 2018, **455**, 705–716.
232 Y. Bao and K. Chen, *Appl. Surf. Sci.*, 2018, **437**, 51–61.
233 Z. Wan, G. Zhang, X. Wu and S. Yin, *Appl. Catal., B*, 2017, **207**, 17–26.
234 T. Ma, J. Wu, Y. Mi, Q. Chen, D. Ma and C. Chai, *Sep. Purif. Technol.*, 2017, **183**, 54–65.
235 H. Huang, K. Xiao, Y. He, T. Zhang, F. Dong, X. Du and Y. Zhang, *Appl. Catal., B*, 2016, **199**, 75–86.
236 H. Huang, X. Han, X. Li, S. Wang, P. K. Chu and Y. Zhang, *ACS Appl. Mater. Interfaces*, 2015, **7**, 482–492.
237 H. Huang, R. Cao, S. Yu, K. Xu, W. Hao, Y. Wang, F. Dong, T. Zhang and Y. Zhang, *Appl. Catal., B*, 2017, **219**, 526–537.
238 L. Zhou, W. Zhang, L. Chen and H. Deng, *J. Colloid Interface Sci.*, 2017, **487**, 410–417.
239 H. Katsumata, T. Sakai, T. Suzuki and S. Kaneco, *Ind. Eng. Chem. Res.*, 2014, **53**, 8018–8025.
240 B. Zhu, P. Xia, Y. Li, W. Ho and J. Yu, *Appl. Surf. Sci.*, 2017, **391**, 175–183.
241 Y. Deng, L. Tang, G. Zeng, J. Wang, Y. Zhou, J. Wang, J. Tang, Y. Liu, B. Peng and F. Chen, *J. Mol. Catal. A: Chem.*, 2016, **421**, 209–221.
242 X. Yang, Z. Chen, J. Xu, H. Tang, K. Chen and Y. Jiang, *ACS Appl. Mater. Interfaces*, 2015, **7**, 15285–15293.
243 Y. Gong, X. Quan, H. Yu and S. Chen, *Appl. Catal., B*, 2017, **219**, 439–449.
244 S. Qin, Y. Lei, J. Guo, J.-F. Huang, C.-P. Hou and J.-M. Liu, *ACS Appl. Mater. Interfaces*, 2021, **13**, 25960–25971.
245 G. Liao, C. Li and B. Fang, *Matter*, 2022, **5**, 1635–1637.
246 Q. Qiao, W.-Q. Huang, Y.-Y. Li, B. Li, W. Hu, W. Peng, X. Fan and G.-F. Huang, *J. Mater. Sci.*, 2018, **53**, 15882–15894.
247 D. Lu, H. Wang, X. Zhao, K. K. Kondamareddy, J. Ding, C. Li and P. Fang, *ACS Sustainable Chem. Eng.*, 2017, **5**, 1436–1445.
248 J. Wang, Y. Xia, H. Zhao, G. Wang, L. Xiang, J. Xu and S. Komarneni, *Appl. Catal., B*, 2017, **206**, 406–416.
249 W.-K. Jo and N. C. S. Selvam, *Chem. Eng. J.*, 2017, **317**, 913–924.
250 F. Wu, X. Li, W. Liu and S. Zhang, *Appl. Surf. Sci.*, 2017, **405**, 60–70.
251 Z. Xie, Y. Feng, F. Wang, D. Chen, Q. Zhang, Y. Zeng, W. Lv and G. Liu, *Appl. Catal., B*, 2018, **229**, 96–104.
252 S. Hua, D. Qu, L. An, W. Jiang, Y. Wen, X. Wang and Z. Sun, *Appl. Catal., B*, 2019, **240**, 253–261.
253 Z. Huang, X. Zeng, K. Li, S. Gao, Q. Wang and J. Lu, *ACS Appl. Mater. Interfaces*, 2017, **9**, 41120–41125.
254 Y. He, L. Zhang, M. Fan, X. Wang, M. L. Walbridge, Q. Nong, Y. Wu and L. Zhao, *Sol. Energy Mater. Sol. Cells*, 2015, **137**, 175–184.
255 Y. Li, S. Tan, Y. Meng, Y. Xia, L. Gao and W. Chen, *J. Mater. Sci.: Mater. Electron.*, 2022, **33**, 13887–13904.
256 D. Li, J. Huang, R. Li, P. Chen, D. Chen, M. Cai, H. Liu, Y. Feng, W. Lv and G. Liu, *J. Hazard. Mater.*, 2021, **401**, 123257.
257 F. Yu, F. Gong, Q. Yang and Y. Wang, *Diamond Relat. Mater.*, 2022, **125**, 109004.
258 A. Sudhaik, P. Raizada, A. A. P. Khan, A. Singh and P. Singh, *Nanofabrication*, 2022, **7**, 280–313.
259 G. Zhao, J. Ding, F. Zhou, X. Chen, L. Wei, Q. Gao, K. Wang and Q. Zhao, *Chem. Eng. J.*, 2021, **405**, 126704.
260 S. Das, T. Deka, P. Ningthoukhangjam, A. Chowdhury and R. G. Nair, *Appl. Surf. Sci. Adv.*, 2022, **11**, 100273.
261 A. Kumar, P. Raizada, P. Singh, R. V. Saini, A. K. Saini and A. Hosseini-Bandegharaei, *Chem. Eng. J.*, 2020, **391**, 123496.

